POLITECNICO DI TORINO

Collegio di Ingegneria Chimica e dei Materiali

Corso di Laurea Magistrale in Ingegneria dei Materiali per l'Industria 4.0

Master's Thesis

The effect of Microcrystalline Cellulose and Lignin on the Physical and Mechanical Properties of Recycled Paper



Supervisor

Prof.Massimo Messori

Candidate

Erfan Khoini

October 2025

Abstract

This research investigates the optimal microcrystalline cellulose (MCC) concentration for OCC-based composite materials which could serve as spray-coated packaging solutions. The main goal focuses on identifying the MCC concentration which optimizes both coating processability through viscosity control and water resistance and compressive strength performance. The OCC paper sheets were produced at the laboratory level before MCC containing formulations were applied through spray coating to semi-wet sheets. The obtained composites underwent complete evaluation through standard testing procedures which included water resistance measurement and compressive strength testing using Cobb60 and Short-Span Compression Test (SCT). The results were compared to literature findings of scanning electron microscopy (SEM) and Fourier transform infrared spectroscopy (FTIR) and x-ray diffraction (XRD) and thermogravimetric analysis (TGA) to study the microstructural, chemical, crystalline and thermal characteristics of the composites.

Higher MCC concentrations up to 10 wt% enhance mechanical properties particularly compressive strength yet they increase viscosity and reduce processability. The MCC concentration exceeds 5 wt% which prevents spraying of the coating. The optimal MCC concentration was found to be 1 wt% because it provided excellent sprayability together with superior water resistance and higher capillary rise and equal mechanical strength to higher concentration levels. These findings demonstrate the importance of achieving material enhancements and process advantages while designing environmentally friendly packaging solutions.

Keywords: Microcrystalline Cellulose (MCC), Old Corrugated Containers (OCC), Spray Coating, Packaging, Composites, Water Resistance, Mechanical Properties, Viscosity, Processability, Cellulose.

1.Introduction	1
2. State of the art	6
2.1. Cellulose	6
2.2. Microcrystalline cellulose	7
2.2.1. Production routes of microcrystalline cellulose	8
2.2.2. Process Variations and Innovations	9
2.2.3. Product Variations and Applications	10
2.3. Cell wall ultra-structure	11
2.4. Nanocellulose	12
2.5. MFC Structure	14
2.6. Papermaking applications	15
2.6.1. Fibers	15
2.6.2. Wood pulps	16
2.6.3. Paper recycling	18
2.7. Coatings and films MFC	19
3. Materials and Methods	20
3.1. Laboratory-Scale Paper Production and Characterization	20
3.2. Pulp Preparation and Storage Protocol for Sheet Formation	23
3.3. Laboratory Handsheet Formation	24
3.3.1. Cobb test	26
3.3.2. Short span Compression Test (SCT)	27
3.4. Integrated Laboratory Process for Handsheet Formation and Semi-Wet Paper Preparation	
3.4.1. Raw Material Preparation	28
3.4.3. System Preparation	29

3.4.4. Drying Procedure	30
3.4.5. Spray coating semi-wet paper sheets	31
4. Results and discussion	32
4.1. Calculation of MCC Percentage in Formulations	32
4.2. Dry Sheet Production and Quality Issues	33
4.3. Semi-Wet Application and Mechanical Testing	35
4.3.1. Properties of MCC Incorporation Semi-Wet Paper Sheets	36
4.3.2. Properties of MFC on Semi-Wet Paper Sheets	38
4.4. SEM characterization	39
4.5. FTIR Characterization	41
4.6. XRD characterization	43
4.8. Density Properties	46
4.8.1. Tensile Performance	46
4.9. Bending Strength Properties	47
5. Conclusion	48
5.1. Implications and Benefits	48
5.2. Limitations and Future Directions	49
6. References	50

Figures

Figure 1. Structure of a cellulose chain, with the cellobiose units indicated in brackets	2
Figure 2. Schematic illustrating the amorphous and crystalline domains of cellulose and hydrogen bonding behavior	3
Figure 4. Schematic representation often wood cell wall ultra-structure	
Figure 5 Schematic representation of latewood tracheid cell wall layers	
Figure 6. Hierarchical levels of cellulose nanomaterials.	13
Figure 7. Structure of cellulose fiber and micro-fibrillated cellulose	. 14
Figure 8. Fiber flocculation by mechanical forces.	. 15
Figure 9. Evolution of fiber bonding configurations, illustrating four flexibility states	17
Figure 10: Evolution of worldwide production of wood pulps	. 18
Figure 11: Standard Cobb test device.	. 26
Figure 12: Clamping with 0,7mm free span (TAPPI T 826 om-08)	. 27
Figure 13: Water Absorption Characteristics of Semi-Wet Paper Sheets with Varying MCC	.36
Figure 14; Water Absorption Rates of MFC Composites at Concentrations from 1% to 10%.	38
Figure 15. SEM image of MCC.	39
Figure 16. SEM micrograph of composite tensile fracture surface with MCC	40
Figure 17. FTIR spectra of cantala/rHDPE composites with varying MCC concentrations	42
Figure 18. XRD patterns of rHDPE and MCC.	. 43
Figure 19. XRD patterns of rHDPE, MCC, and cantala/rHDPE composites with varying MCC) .
	. 44
Figure 20. Density and Tensile Strength Variations in MCC-Reinforced Composites	46
Figure 21. Bending Strength of MCC-Reinforced rHDPE/Cantala Composites	47

Tables & Photos

Table 1: Standard Acid Hydrolysis Conditions for MCC production	9
Table 2: Microcrystalline Cellulose (MCC) Product Variations and Commercial Applications .	10
oic1: Old Corrugated Containers (OCC)	20
pic2: IDM Test Laboratory Disintegrator	20
pic 3: RK-2A Rapid Köthen Sheet Former	21
pic4: cylindrical tank of the RK machine	21
pic 5: Climate-controlled chambers maintaining 50±2% RH or 90±2% RH	22
pic 6: The paper was cut to a standard size for testing	23
pic 7: Short span Compression Test compression test	28
Table 3: Dry solid percentage of materials	29
pic 8: Oven Curing	30
oic 9: a water-based gel containing microcrystalline cellulose (MCC)	32
Table 4:, MCC test results for cobb & sct	34
pic 10: cobb test of the dry sheet	34
pic 12: Water Absorption Characteristics dry sheet	34
Table 5: result of test of MCC for cobb & sct percentages (1-10%)	35
Table 6: Evaluation of Microcrystalline Cellulose (MCC) Performance Across Key Sheet	
Properties	37

1.Introduction

Although the reinforcement potential of microcrystalline cellulose (MCC) is well-established, the optimal concentration for spray-coated packaging applications remains uncertain. This thesis investigates MCC concentrations (1–10 wt%) in composites with old corrugated containers (OCC) to achieve an optimal balance between processability (e.g., viscosity) and mechanical performance [1]. Given the structural similarities between MCC and native cellulose, understanding the structural properties of native cellulose is essential. These properties, particularly the crystalline characteristics of cellulose, vary significantly depending on the source species and processing treatments [2].

The crystalline attributes of cellulose profoundly influence the MCC properties. For example, the length of cellulose crystals is hypothesized to correlate with the level-off degree of polymerization (DP), which is a topic explored in subsequent chapters. This section examines the crystalline properties of cellulose impact on MCC products. [2]

Cellulose constitutes one-third to two-thirds of plant material by weight, with tree-derived cellulose typically ranging from 40 to 47 wt%. It can be isolated via various pulping processes. Owing to its excellent network-forming capabilities and abundant availability, cellulose fibers are widely used in producing diverse materials. [3]

Cellulose is an unbranched polysaccharide comprising β -1,4-glycosidically linked D-glucopyranose units, with a degree of polymerization (DP) ranging from 2,000 to 15,000. MCC shares this bonding structure but exhibits a reduced DP. During bond formation, each linkage between glucose units releases one water molecule, and adjacent units are rotated 180° within the plane. [4]

Structurally, cellulose can also be regarded as a cellobiose polymer, where each cellobiose unit comprises two anhydro glucose molecules with oppositely oriented free hydroxyl groups.

Collectively, these units form the isotactic monomer unit of cellulose. [5]

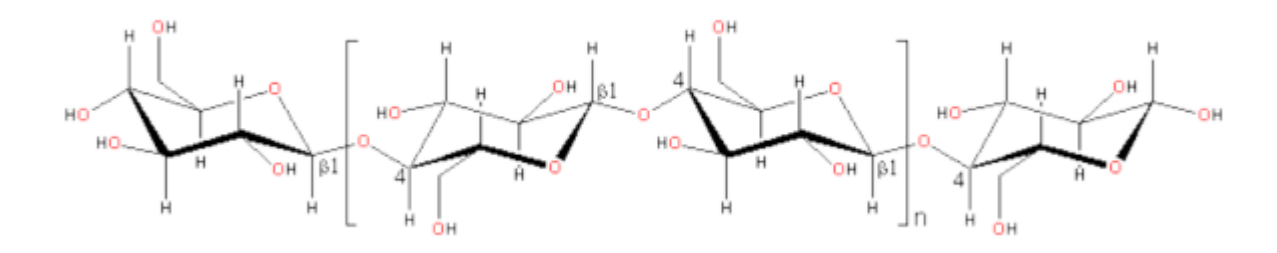


Figure 1. Structure of a cellulose chain, with the cellobiose units indicated in brackets [6].

Crystallinity values are challenging to compare across studies due to differences in treatment processes and measurement techniques. For instance, results from cross-polarization magicangle spinning nuclear magnetic resonance (CPMAS-NMR) and X-ray diffraction (XRD) are not directly comparable, and even XRD measurements may vary significantly between investigations. In MCC production, crystallinity values exhibit wide variability but often approximates the original cellulose feedstock. [6]

The impact of hydrolysis on crystallinity is still debated, although a slight increase is commonly proposed. For example, Leppänen et al. (2009) observed an increase from 50% to 63% when converting kraft pulp into MCC. Additionally, Zabler et al. (2010) suggested that moisture fluctuations and tensile stress may induce fibril deformations, further influencing crystallinity [6].

Crystalline regions can be isolated to yield either MCC or cellulose nanocrystals (CNCs). The production processes of these materials are detailed in the next chapter. Figure 2 illustrates the amorphous and crystalline domains of cellulose, alongside its hydrogen-bonding structure. [7]

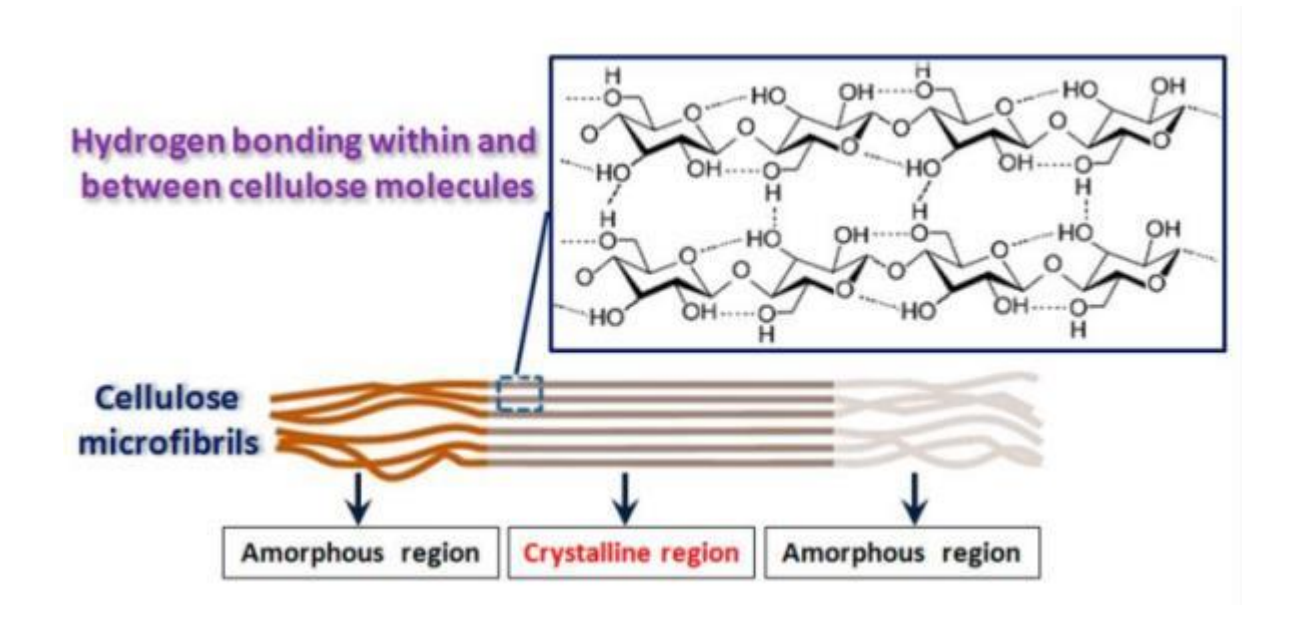


Figure 2. Schematic illustrating the amorphous and crystalline domains of cellulose and their hydrogen bonding behavior [8].

Cellulose's crystalline domains arise from a complex network of interchain and intrachain hydrogen bonds. Variations in these bonding patterns produce seven distinct crystalline allomorphs. Naturally occurring cellulose I exists in two forms: I α , which is predominant in algae and bacteria, and I β , the primary form in plants. Harsh treatment conditions or hydrothermal modification can shift the I α /I β ratio, typically increasing the I β proportion. In this study, plant-derived cellulose, unexposed to conditions altering its polymorphism, is assumed to consist solely of the I β allomorph [δ].

Additional allomorphs (II, III, and IV) result from processing native cellulose or its refined derivatives. Notably, cellulose II, widely regarded as the most thermodynamically stable form, holds significant commercial importance; however, some studies suggest that cellulose I may possess a lower energy state. Conversion from cellulose I to II typically occurs via mercerization or regeneration in alkaline systems (≥5 N NaOH). Under mild acid treatment, cellulose retains its native Iβ structure [9].

The microcrystalline cellulose (MCC) investigated here, consistent with most commercial MCC, comprises allomorph I [9]. Emerging research explores alternative allomorphs, such as cellulose II-based MCC, for enhanced properties such as improved water disintegration and pelleting performance in pharmaceutical applications. Detailed discussions on allomorph properties and reactivity are available in specialized literature [10].

Cellulose exhibits a hierarchical structure spanning molecular to macroscopic scales, as depicted in Figure 3:

1. **Molecular**: β -1,4-glycosidic chains \rightarrow cellobiose units

2. **Supramolecular**: Elementary fibrils (1.5–3.5 nm) → microfibrils (10–30 nm) 3.

Macroscopic: Fiber networks → cell wall layers (S1–S3).

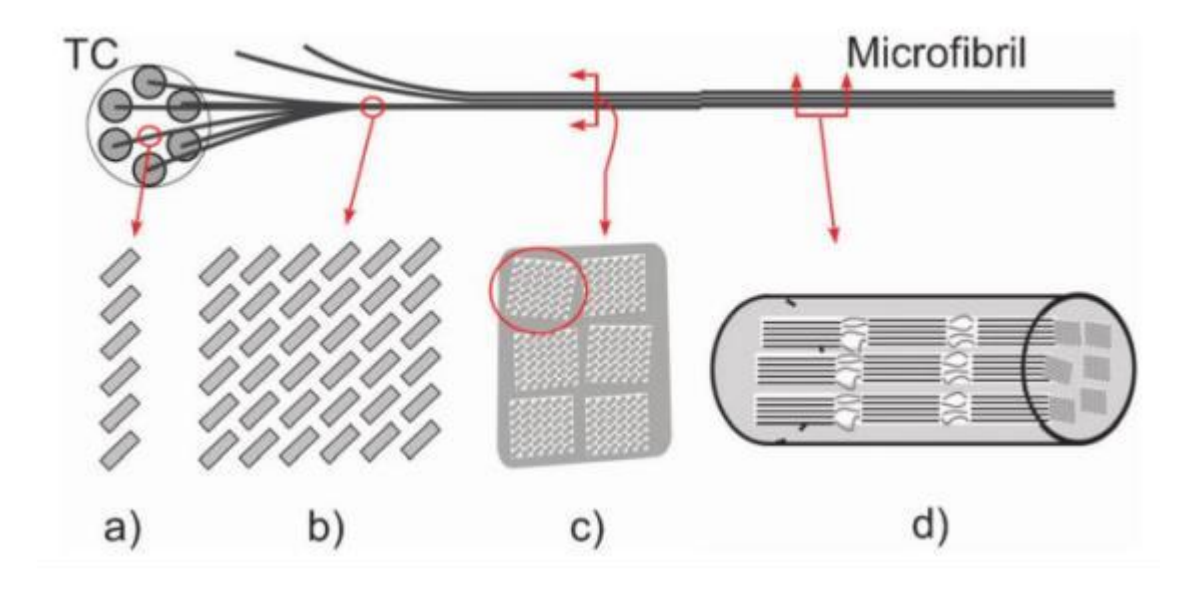


Figure 3. Hierarchical structure of wood fiber cellulose [11].

nomenclature of these structural levels is defined in subsequent sections. Figure 3 provides a schematic of the fiber architecture:

(a) Linear assembly of six cellulose chains synthesized by a single cellulose synthase rosette subunit. (b) Elementary fibril (6×6 cellulose chains), produced by the cellulose synthase complex. (c) Microfibril, composed of aggregated elementary fibrils. (d) Cellulose chain with alternating crystalline (straight) and amorphous (curved) domains. In Figure 3, each gray box represents an individual cellulose chain. MCC predominantly comprises the crystalline regions of these chains after the removal of amorphous segments [11].

The structural organization of elementary cellulose fibrils remains a subject of ongoing research. Current evidence indicates that plant-based elementary fibrils consist of 18–36 cellulose chains, exhibiting an asymmetric cross-section with dimensions of 2.9–5.3 nm. The prevailing hypothesis suggests that the terminal enzyme complex, which is responsible for the simultaneous synthesis of multiple chains, governs this structure [12].

The terminal enzyme complex likely determines the elementary fibril structure, with 36-chain configurations being prevalent in plants and trees [13].

Microfibrils form through the bundling of elementary fibrils, and their size varying by cellulose source. These fibrils are not composite structures composed of hemicellulose; instead, they aggregate via extensive hydrogen bonding to form microfibrils [13]. Typically embedded in a hemicellulose matrix, microfibrils may comprise one or multiple elementary fibrils in cross-section [14]. MCC production partially separates this matrix while preserving the crystalline microfibril regions.

At the ultrastructural level, the cell walls feature distinct composite matrices. The primary wall exhibits less ordered organization, with components such as hemicellulose and lignin deposited on the middle lamella. Conversely, the secondary wall, typically comprising two or three layers, contains parallel cellulose chains that enhance structural reinforcement through distinct alignment patterns [15].

Although the precise structure of elementary fibrils remains uncertain, current models propose that cellulose-synthesizing rosettes, coordinated by microtubules, align within the cell wall. These microtubules and associated proteins regulate cellulose synthesis and spatial orientation, forming linear arrays of elementary fibrils [16].

2. State of the art

2.1. Cellulose

Cellulose is the primary structural component of wood, typically accounting for 40%–45% of dry mass across most species. The remainder comprises hemicellulose (20–30%), lignin (20–35%, varying by species), and minor extractives (typically <10%). Structurally, cellulose exists in two morphological phases: crystalline regions with highly ordered molecular arrangements and amorphous regions with disordered organization. This duality fundamentally governs the mechanical properties of natural fibers, and the proportions and spatial configuration of these regions critically influencing material performance [17].

At the molecular level, cellulose exhibits a complex hierarchical organization. The fundamental units, elementary fibrils, measure 1.5–3.5 nm in width and approximately 100 nm in length. These aggregate into larger microfibrils (10–30 nm wide), which further assemble into microfibrillar bands approximately 100 nm wide and extending to micrometer-scale lengths. Within plant cell architecture, this cellulose network predominantly resides in the secondary cell wall and exhibits consistent structural organization across species [18]. The cell wall comprises multiple layers: the middle lamella (ML), which binds adjacent cells; the thin primary wall (P); and the substantial secondary wall, which is subdivided to three sublayers (S1, S2, S3). The S2 layer, the thickest at 2–4 µm, contains most cellulose microfibrils, while the innermost warty layer (W) completes the structure [19].

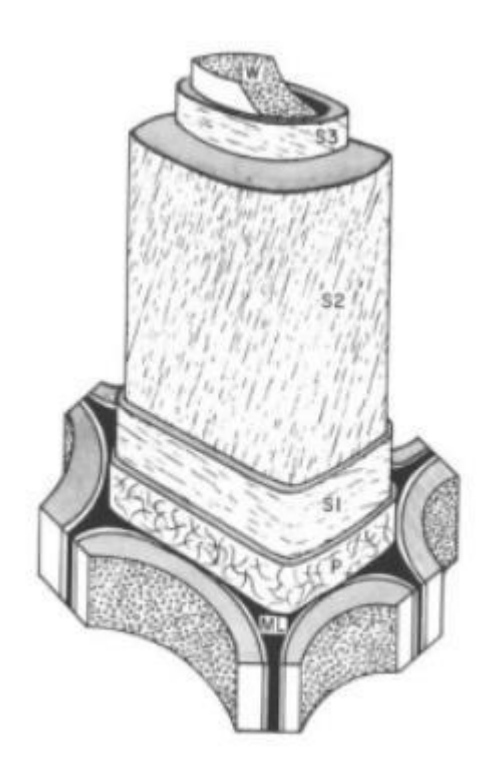


Figure 4. Schematic representation often wood cell wall ultra-structure, illustrating the characteristic layers: middle lamella (ML), primary wall (P), secondary wall (S1, S2, S3), and warty layer (W). The S2 layer, the thickest portion, harbors most cellulose microfibrils [19].

2.2. Microcrystalline cellulose (MCC)

MCC is produced via mild acid hydrolysis of α-cellulose, yielding a material with a significantly reduced degree of polymerization (DP) compared to native cellulose. Conventional production involves acid treatment at elevated temperatures, typically 100°C (boiling point) or 121°C (pressurized conditions) [20]. Hydrolysis is effective across a broad range of acid concentrations, producing MCC with slightly varying properties. Alternative methods, such as high-shear extrusion using reactive oxygen species, hydrolyze cellulose into microcrystalline dimensions at 80–200°C [20,21].

During hydrolysis, crystalline regions remain largely intact or experience minimal surface damage, whereas amorphous domains dissolve preferentially. This selectivity arises from the tightly packed crystalline structure, which restricts the penetration of water and hydrogen ions.

According to FAO standards (2015), MCC must contain ≥97 wt.% carbohydrate content (dry basis) with a degree of polymerization generally below 400. For food applications, additional

specifications apply: ≤10 wt.% of particles with diameter <5 µm, along with restrictions on solubility, water absorption, drying loss, and impurities [21]. Pharmacopeial standards are more stringent, requiring a DP below 350 [22].

2.2.1. Production routes of microcrystalline cellulose

The modern production process for MCC was pioneered in the 1950s by Battista and colleagues [23]. The foundational method described in Battista's patents involves hydrolyzing amorphous cellulose domains using either:

- 1. 2.5 N hydrochloric acid at boiling temperature (100°C) for 15 minutes, or
- 2. 0.14 N hydrochloric acid at 121°C for one hour

Post-hydrolysis, the material is washed, optionally dried, and subjected to mechanical or high-pressure disintegration to form stable colloidal dispersions or gels. [23,24] The stability is primarily due to the controlled particle size distribution. The final product was fractionated via mechanical sifting and dried

Key characteristics of this process include the following:

- 1. Approximately 90% reduction in content due to dissolution of inorganic components in amorphous regions.
- 2. Final product purity ranging from 95%–99% glucose content.
- 3. Establishment of the first commercial MCC product [25].

2.2.2. Process Variations and Innovations

Although most MCC production follows a basic acid hydrolysis framework, several innovative variations have emerged [26]:

1. Optimized Acid Hydrolysis:

- A 1% sulfuric acid (H₂SO₄) solution.
- Enhances yields through optimized pulping techniques.
- Minimizes particle aggregation.

2. Steam Explosion Techniques:

Facilitate byproduct recovery (e.g., hemicellulose, lignin, glucose).

- Ha and Landi's method enhance pharmaceutical and food applications as follows:
- Employing optimized steam parameters.
- Incorporating hydrophilic attrition aids (e.g., carboxymethylcellulose).
- Producing more uniform colloids [26].

Parameter	Battista Method	Optimized Method	Steam Explosion
	(HCI)	(H_2SO_4)	
Acid Concentration	2.5-N HCl or 0.14 N HCl	1% H ₂ SO ₄	N/A (Steam + attrition aids)
Temperature	100°C (boiling) or 121°C (pressurized)	80-100°C	160-200°C
Time	15 min (100°C) or 1 h (121°C)	30-60 min	5-10 min
Key Outcomes	DP < 400, 95-99% glucose purity	Higher yield and reduced aggregation	Byproduct recovery (hemicellulose/lignin)

Table 1: Standard Acid Hydrolysis Conditions for MCC production [26-27].

2.2.3. Product Variations and Applications

Modern MCC products primarily vary in three respects:

- 1. Particle size distribution
- 2. Moisture content
- 3. Additive composition [28]

Variation Parameter	Typical Specifications	Impact on Properties	Example Products (Avicel® Grades)	Primary Applications
Particle Size Distribution	20–200 μm (grade- dependent)	Flowability Compressibility Dissolution rate	PH-101 (50 μm) PH-200 (180 μm)	Pharmaceutical tablets Food thickeners
Moisture Content	3%–5% (pharma grades)5–8% (food grades)	StabilityProcessing behavior	PH-102 (≤5%) DG (≤8%)	Wet granulation Baked goods
Additive Composition	None (pure MCC) CMC blends Silica coatings	Binding capacity Lubricity Disintegration time	PH-113 (silicified) RC-591 (CMC blend)	Direct- compression tablets Instant foods
Variation Parameter	Typical Specifications	Impact on Properties	Example Products (Avicel® Grades)	Primary Applications

Table 2: Microcrystalline Cellulose (MCC) Product Variations and Commercial Applications [28].

2.3. Cell wall ultra-structure

In softwoods, tracheids comprise over 90% of the total cell volume, with parenchyma cells forming the remainder. These elongated, narrow, and hollow fibers serve as the primary structural units of softwood tissue [29]. As shown in Figure 5, the tracheid cell wall features a distinct layered structure: the outermost middle lamella (ML) binds adjacent cells, while the hollow lumen forms the interior space. The cell wall includes a thin primary wall (P) and a thicker secondary wall, which is subdivided into three sublayers: S1 (outer), S2 (middle), and S3 (inner). The S2 layer is the thickest component of the secondary wall [30].

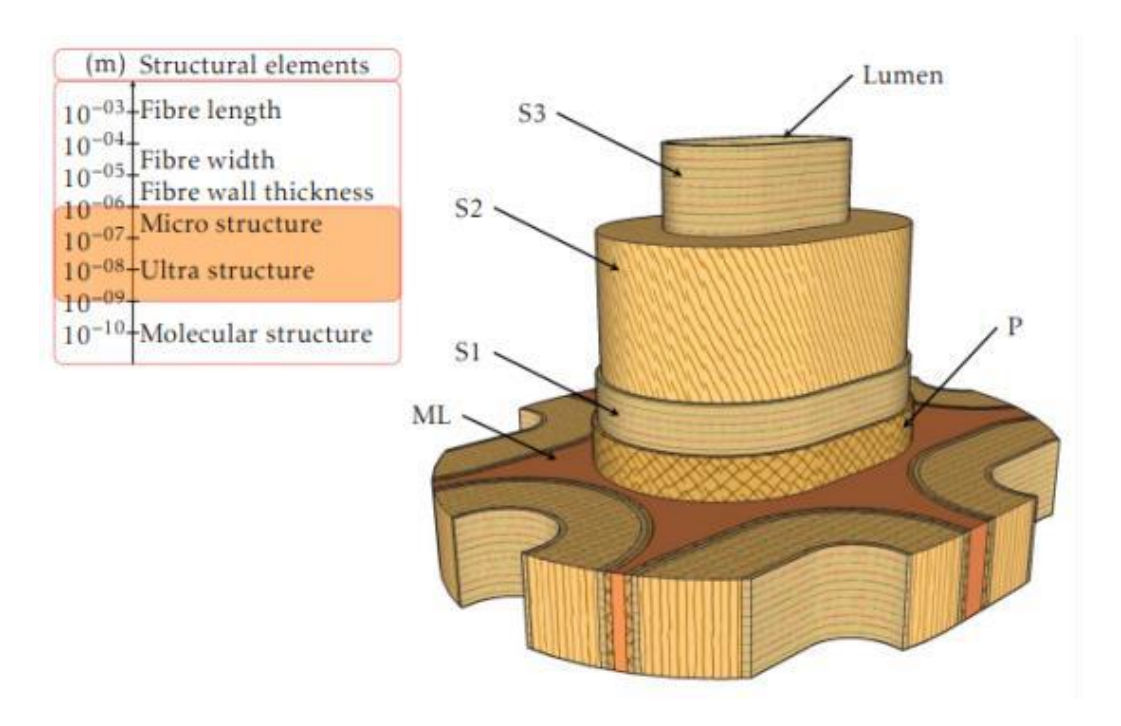


Figure 5 Schematic representation of latewood tracheid cell wall layers [30].

The secondary wall primarily comprises cellulose with minor lignin and hemicellulose content. The S1 and S3 layers, ranging from 0.1–0.3 µm in thickness, exhibit homogeneous, rigid structures [30].

The S2 layer varies significantly between the earlywood (EW) and latewood (LW) tracheids. The EW tracheids, it measures approximately 1 μ m thick, whereas in LW tracheids, it reaches about 5 μ m. This variation accounts for the thinner cell walls and wider lumens in EW tracheids than in LW tracheids [31].

2.4. Nanocellulose

Nanocellulose denotes cellulosic materials with at least one dimension in the nanoscale range (1–100 nm), as defined by TAPPI WI-3021. This category includes three primary types differentiated by production methods and structural traits [31]:

- 1. Cellulose Nanofibrils (CNFs)
- 2. Cellulose Nanocrystals (CNCs)
- 3. Bacterial Nanocellulose (BNC)

Terminology in the literature varies. CNFs are often termed nanofibrillated cellulose (NFC) or micro-fibrillated cellulose (MFC), while CNCs may be labeled nanocrystalline cellulose (NCC) or cellulose whiskers, reflecting evolving nomenclature in the field [32].

Figure 6 illustrates the dimensional properties across hierarchical levels:

- CNFs: Diameters of 20–40 nm, lengths extending to several micrometers.
- CNCs: Widths of 2–20 nm, lengths of 100–600 nm up to micrometer-scale.
- BNC: Microfibrillar bands 20–100 nm wide, composed of elementary nanofibrils 2–4 nm in diameter [33]-[34].

This structural diversity highlights the unique morphological characteristics achievable through distinct production methods, each tailored to specific applications [34].

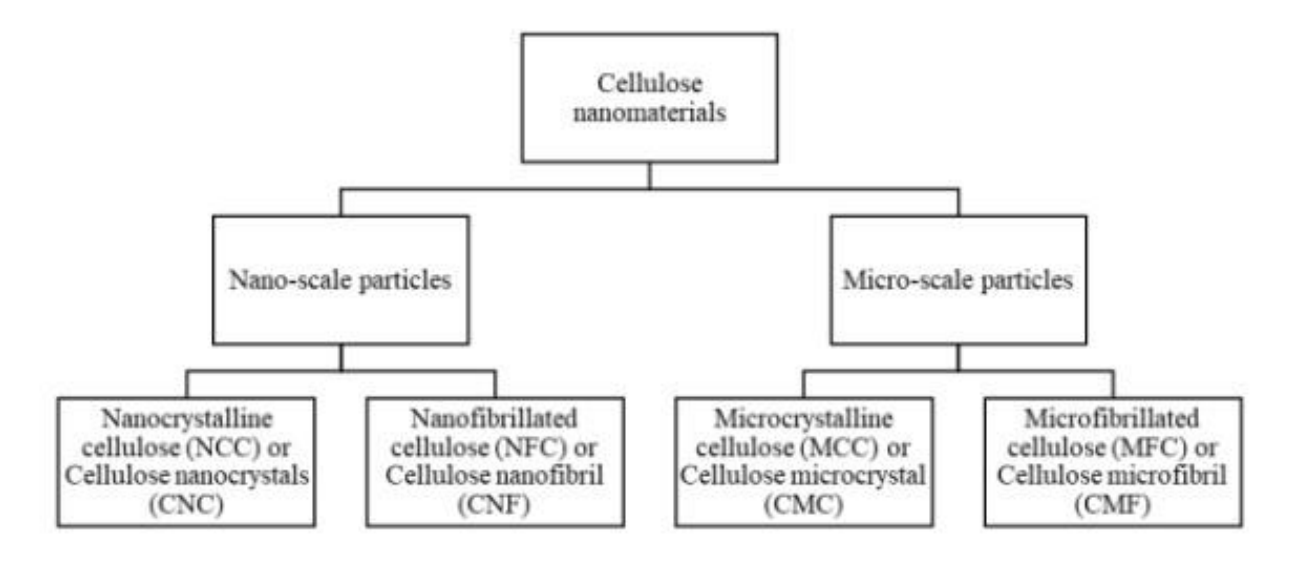


Figure 6. Hierarchical levels of cellulose nanomaterials [34].

The mechanical production of CNF was pioneered by Herrick and Turbak using high-pressure homogenization. This work spurred the development of alternative methods such as grinding and micro fluidization. Conversely, CNCs are typically produced via acid hydrolysis, selectively dissolving amorphous regions while retaining the crystalline domains. Sulfuric acid is particularly effective in yielding needle-like nanocrystals with dimensions influenced by cellulose source, hydrolysis conditions, and ionic strength [35].

These methods confer distinct properties. CNC exhibit high crystallinity (62–90%), reducing flexibility compared to more pliable CNF [35]. BNC, biosynthesized by microorganisms, forms a gel-like material with exceptional mechanical properties due to its nanostructure. The high specific surface area and porosity enhance mechanical endurance, hydrophilicity, and water retention [36].

2.5. MFC Structure

MFC has a heterogeneous structure, encompassing microscale components (fiber fragments, fibers) and nanoscale elements (nanofibrils, fibrillar fines). When optimally processed, nanofibers are predominant. Mechanical production applies high-shear forces, splitting cellulose fibrils longitudinally along their axis, resulting in MFC's characteristic high specific surface area [37].

Typical MFC fibrils measure 20–60 nm in diameter and extend to several micrometers in length. Their flexibility facilitates an interconnected web-like network, distinguishing MFC from other nanocellulose forms [38]. Unlike CNC, which are purely crystalline, MFC retains both amorphous and crystalline regions, contributing to its unique mechanical and interfacial properties [38].

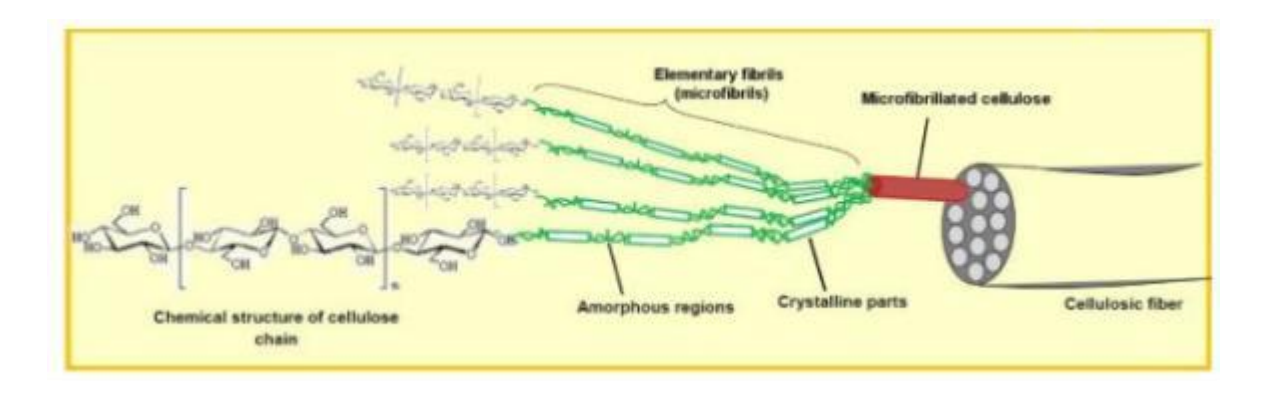


Figure 7. Structure of cellulose fiber and micro-fibrillated cellulose [38].

2.6. Papermaking applications

2.6.1. Fibers

Wood fibers feature spirally arranged cellulose fibrils. Fiber flocculation in suspensions occurs via two primary mechanisms:

1. Mechanical Forces:

- Mechanical linking: Prevents relative movement between fibers through surface roughness and irregular morphology, creating spatial variations in the fiber mass distribution [39].
- *Elastic interlocking*: Maintains fiber position is maintained through frictional forces and multi-point contact (minimum three contact points), holding fibers in strained configurations [39].

2. Colloidal Forces

Figure 8 shows that these mechanical interactions predominate in high-consistency suspensions with high-aspect-ratio fibers. Mechanical linking excels with coarse-surfaced fibers, whereas elastic interlocking relies on the fiber network's deformation properties [40].

.

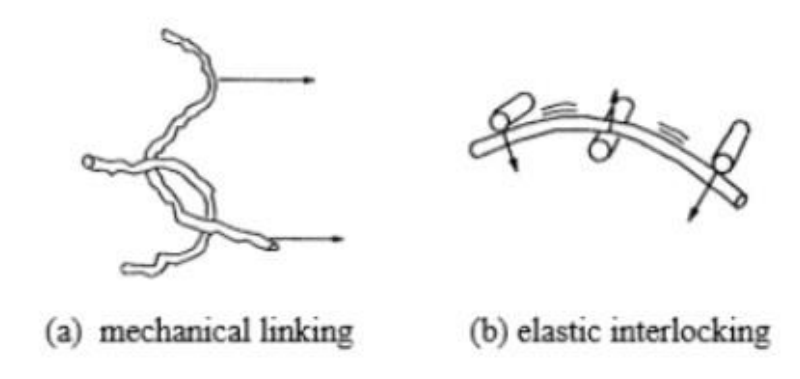


Figure 8. Fiber flocculation by mechanical forces (a) mechanical linking and (b) elastic interlocking [40].

2.6.2. Wood pulps

Wood is the primary raw material for pulp production, although non-woody annual plants are also used in wood-scarce regions. The manufacturing process comprises the following key stages [41]:

1. Raw Material Preparation:

- I. Debarking of wood logs
- II. Chipping into uniform pieces
- III. Storage and conditioning of chips

2. Pulping Methods:

- A. Chemical pulping:
- I. Alkaline process
- II. Sulfite processes (acid bisulfite, bisulfite, neutral sulfite, alkaline sulfite)
- III. Alternative methods (e.g., nitric acid, organic solvents/acids)

Kraft pulping outperforms sulfite processes in yielding superior mechanical properties. During chemical digestion, removal of lignin and hemicellulose from lignocellulosic materials enhances fiber characteristics [42].

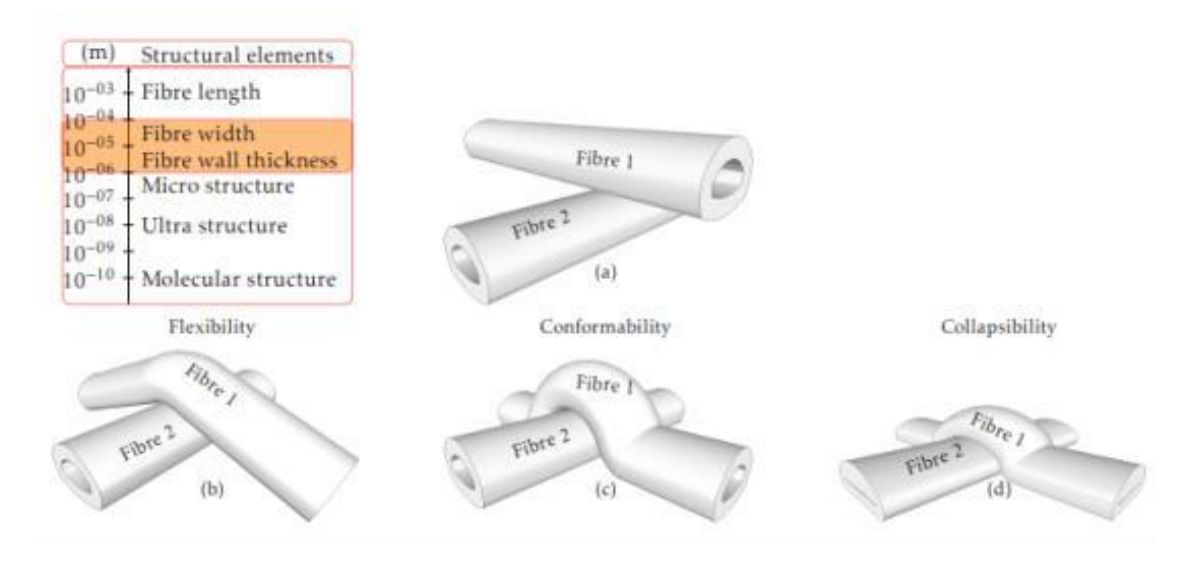


Figure 9. Evolution of fiber bonding configurations, illustrating four flexibility states: (two rigid fibers with minimal contact, (b) partial compliance with one flexible fiber conforming to a rigid one, (c) asymmetric adaptation with a highly conformable fiber, (d) complete mutual collapsibility maximizing contact area through full flexibility [43].

Fiber properties—collapsibility, conformability, flexibility, coarseness, shape, and fibrillation—fundamentally shape fiber network characteristics. These traits depend on the fiber wall's chemical composition and morphology. Pulping dissolves lignin and hemicellulose, creating a porous fiber wall architecture in which the pore size inversely correlates with pulp yield [43]. Greater removal (lower yield) increases porosity, enhancing fiber conformability and collapsibility during network formation. This modification enhances inter-fiber bonding while affecting network density, strength, and light scattering. The interplay between pore structure and flexibility significantly governs the conformability of sheets during sheet formation and processing [44].

2.6.3. Paper recycling

Global wood pulp utilization by sector, highlighting current distribution and future trends. Approximately 95% of wood pulp production currently supports traditional applications, with 5% allocated to the chemical industry. Emerging biorefinery technologies are expected to shift this distribution, creating new value chains for wood-based chemicals and materials [45]. This projected growth in chemical sector use reflects advances in lignocellulosic biomass conversion and the rising demand for sustainable alternatives to petroleum-derived products [46].

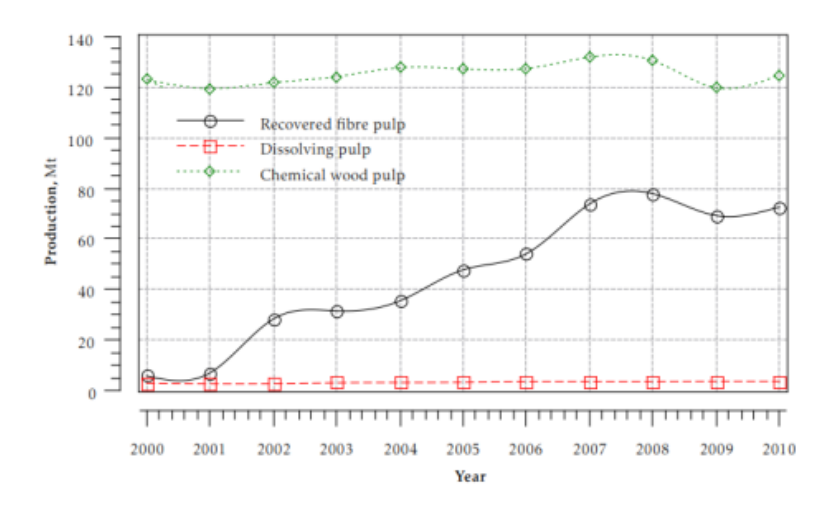


Figure 10: Evolution of worldwide production of wood pulps [47].

The paper recycling process encompasses resulting/disintegration, deinking, washing, refining, pressing, and drying. Refining, pressing, and drying modify fiber characteristics, whereas the other stages minimally of the morphological [47]. Recycled fibers typically exhibit lower strength, swelling capacity, and optical properties compared to virgin fibers. Advanced recycling technologies, such as improved deinking and mechanical refining, can partially restore fiber quality by removing contaminants and regenerating surface fibrils. Modern papermaking equipment mitigates quality deterioration by enhancing the sheet strength and surface properties, albeit often at higher production costs [47-48].

Wastepaper is categorized based on origin, quality, and intended use. Pre-consumer waste originates from paper-converting plants, while post-consumer waste is collected from retail establishments, offices, and households [48].

The four primary classifications of wastepaper are:

- Pulp substitutes: High-quality materials, including converting and printing trimmings
- 2. **Deinking grades**: Printed materials such as newspapers (ONP), magazines (OMG), and office papers (CPO, MOW, OMP, SOP)
- 3. **Brown kraft grades**: Packaging materials, including corrugated containers (OCC), kraft sacks, and related converting waste
- 4. **Mixed wastepaper (MWP)**: Materials not suitable for the above categories [49]

2.7. Coatings and films MFC

MFC as a coating additive for paper and cardboard packaging is gaining attention in European Union initiatives for eco-friendly solutions. This sustainable alternative to petroleum-based polymers enhances material performance while reducing environmental impact [50].

MFC coatings fulfill two primary packaging functions:

- 1. Surface quality enhancement (improved printability and surface characteristics)
- 2. Barrier property modification (water vapor, oxygen, grease, and oil resistance)

Subsequent studies have further elucidated MFC's performance characteristics:

- Lavoine observed substantial mechanical property improvements in MFC-coated cardboard, although the barrier properties showed limited enhancement
- Ankerfors reported remarkable mechanical enhancements in MFC composites, including the following [51]:
 - 1. 50% increase in the tensile strength
 - 2. 226% improvement in strain at break
 - 3. 61% enhancement of Young's modulus

These findings underscore MFC's potential as multifunctional coating material, addressing both sustainability and performance demands in packaging. The unique nanostructure enables property combinations unattainable with conventional coatings, positioning MFC as a promising solution for next-generation eco-efficient packaging [52].

3. Materials and Methods

3.1. Laboratory-Scale Paper Production and Characterization

Pulp preparation begins with weighing 30 g dry fibers, with ~8 % moisture of OCC using an analytical balance (±0.01 g accuracy). This material is mixed with tap water in a vessel to form a 1.5% consistency slurry (total mass 2 kg). The slurry was processed in an IDM Test Laboratory Disintegrator (Picture 2) at 30,000 rpm for 10 minutes to ensure complete fiber separation. The resulting suspension was transferred to a 12 L mixing tank, diluted to 0.314% consistency (total mass 9550 g), and homogenized at 1500 rpm for 15 minutes to achieve uniform fiber distribution.



pic1: Old Corrugated Containers (OCC)



pic2: IDM Test Laboratory Disintegrator

For sheet formation, 1,150 g slurry (approximately 3.6 g oven-dried fiber) is introduced into the RK-2A Rapid Köthen Sheet Former (Picture 3). The process starts by filling the cylindrical tank (Picture 4) with 4 L of deionized water at 23±1°C, followed by adding the slurry. The volume is adjusted to 8 L, and a vacuum (18 inHg) drains water through the forming wire for 120 seconds.



pic 3: RK-2A Rapid Köthen Sheet Former



pic4: cylindrical tank of the RK machine

Through a 200-mesh forming wire, yielding an even fiber mat. A pH-neutral blotting paper (90 g/m²) is applied before transferring the wet web to a hydraulic press, where 2 bars for 2 min pressure is exerted for five minutes, achieving 45±5% solids content. The sheets were dried in Rapid Köthen driers for 7 min under vacuum, then conditioned in a convection oven at 105°C for 60 minutes to attach and spread the lignin solution to the fibers.

Coatings were applied using an airbrush system (0.5 mm nozzle) with lignin solution (12% solids content). The paper substrate, mounted on a drum rotating at 30 rpm, undergoes three uniform spray passes from 20 cm at 200 kPa atomizing pressure, targeting a coat weight of 5±0.5 g/m². Coated sheets are thermally cured in the RK oven at 105±1°C for 60 minutes to ensure solvent evaporation and polymer cross-linking.

Specimens were conditioned for at least four hours in climate-controlled chambers (Picture 5) at 23±1°C and either 50±2% RH or 90±2% RH, with weights monitored hourly to confirm moisture equilibrium. Water resistance is assessed via a modified Cobb60 test: samples are secured under a 10-cm-diameter stainless steel ring with water volume equals 1 cm high water column on top of the specimen (23°C) for 60 seconds. Post-exposure, samples were blotted with absorbent paper (two passes) and weight gain is measured using a precision balance (±0.001 g), normalized by area [53].



Pic 5: Climate-controlled chambers maintaining 50±2% RH or 90±2% RH.

The IDM Test Short-Span Compression Tester (SCT-07), with 15-mm-wide clamps and 0,3 mm for thin paper, 0,7 mm for regular gauge length, evaluates mechanical properties. Samples are tested at two mm/min crosshead speed under controlled conditions (23°C, 50% RH), with data recorded at 100 Hz. The compressive strength is derived from peak force.



pic 6: The paper was cut to a standard size for testing.

3.2. Pulp Preparation and Storage Protocol for Sheet Formation

Pulp preparation for sheet formation requires strict adherence to standardized procedures to ensure experimental consistency. The recycled paper must be processed within seven days of repulping to prevent fiber degradation. Preparation starts by measuring the paper substrate's dry content using a Kern Moisture Analyzer, then calculating the quantity needed for a 5% consistency suspension. For METNIN™ SHIELD experiments, 3000-g pulp per substrate type is prepared, matching the heat mixer's maximum capacity.

Assuming 92% dryness, 163 g of paper is manually torn into pieces ($<5 \times 5$ cm) to preserve fiberlength integrity, as mechanical cutting could impair fiber structure and experimental results. The torn paper is mixed with tap water to achieve a total mass of 3000-g. For repulping-resistant grades, presoaking in warm water ($40-45^{\circ}$ C) for 4-24 hours aids fiber separation. Repulping uses a sealed heat mixer with a whisker attachment and a rubber-gasketed lid to minimize evaporation [54]. The protocol involves a 15-minute initial mix at speed setting two, manual removal of adhered fragments, and a final 10-minute mix for complete dispersion.

Approximately 8%–10% of water is lost to evaporation and absorption during processing. The pulp is aliquoted into pre-weighed plastic containers, each holding 600-g of suspension (30 g dry fibers), yielding four full batches and a fifth partial batch (550–570 g) due to process losses.

Dry and wet pulps must be shielded from light and heat, with wet aliquots stored airtight at 4±1°C to prevent moisture loss and microbial growth. The pulpe should be used within seven days of repulping to preserve fiber properties and suspension integrity.

Containers are labeled with the preparation date, pulp type, and consistency for inventory management. Regular checks—consistency measurements and visual inspection for contamination—validate pulp suitability during storage [55].

3.3. Laboratory Handsheet Formation

The handsheet formation process requires precise calculation of pulp volume based on suspension consistency (0.314% standard) and target basis weight (typically 110-115-g/m²). For accurate results, operators should first produce a reference sheet to account for the potential mass loss from water-soluble components, adjusting subsequent volumes accordingly. The RK system's automated operation involves several critical preparation and processing stages:

System Preparation

- **Preheating**: Initiate the startup system at least 45 minutes before use, allowing the water bath to stabilize at 92-93°C.
- Quality checks: The water pressure (maintain 2.5-3 bar) and circulation pump operation were verified.
- Component inspection: The clean condition of the 200-mesh forming wire and proper alignment of the former column.

Automated Formation Sequence

The RK processor executes the following six sequential phases with electronic monitoring:

- 1. **Filling Phase**: Gradual water introduction into the column (4L initial volume for pulp addition, 7L final volume).
- 2. **Agitation Phase**: 30-second mechanical mixing at 120 rpm for uniform fiber distribution.

- 3. **Calming Phase**: 60-second quiescent period for fiber orientation.
- 4. **Dewatering**: Gravity drainage through the formation of a wire (120 seconds)
- 5. **Accelerated Dewatering**: Vacuum-assisted drainage (40 kPa for 90 seconds)
- 6. Final Suction: High-vacuum extraction (80 kPa for 30 seconds)

When water is drained from the column and draining is complete, the operator unlocks the shafts on both sides of the sheet former column and opens the column by lifting it from the handle. An unused carrier board is placed on top of the formed sheet. Excess water is pressed out by rolling a couching roll on the sheet and board twice back and forth perpendicularly. Wire is lifted from the column with the formed sheet and carrier board attached to it, turned around, and gently hit onto the soft rubber plate placed on the sheet former table in order to detach the formed sheet. The wire is then taken to the sink, gently rinsed with water from the underside, and brought back to the column, which is closed.

3.3.1. Cobb test

The Cobb test was used to evaluate the water absorption properties of paper under controlled conditions. Specimen preparation involves cutting 285 mm diameter circular samples per test sheet with a calibrated cutter, conditioning them at $23\pm1^{\circ}$ C and $50\pm2\%$ RH for at least four hours, and recording their initial dry mass (W₀) to ±0.001 g using an analytical balance.

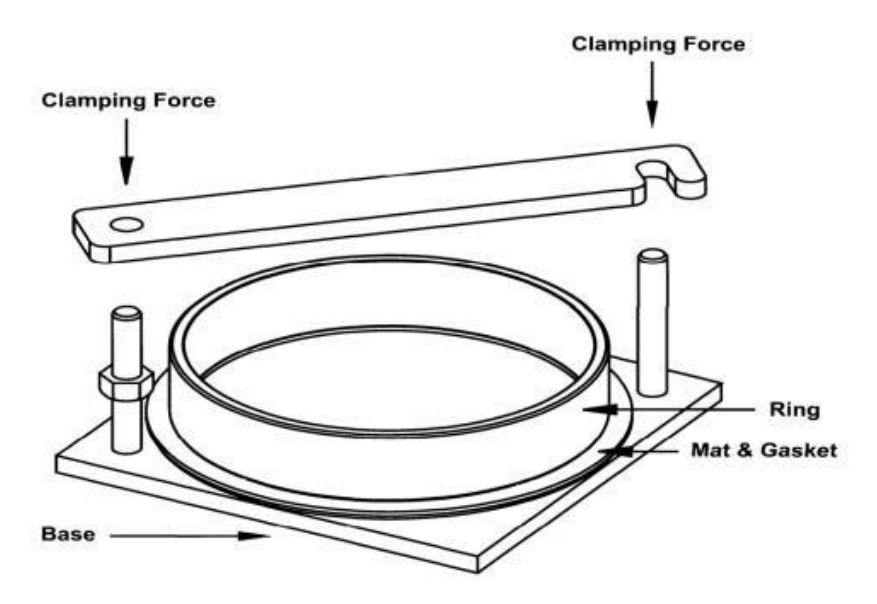


Figure 11: Standard Cobb test device.

Quality control entails monitoring water temperature every five tests, monthly checks of cylinder sealing pressure, documenting leaching via colorimetric analysis of residual water, fiber transfer on blotting papers, and coating integrity. For extended tests (Cobb120, Cobb300), additional humidity controls were applied, rejecting specimens with edge wicking or seal failure. The protocol mandates balance calibration before each series and continuous ambient condition logging to maintain results within ±2% tolerance [56].

The Cobb value using:

$$\text{Cobb}_{60} = (W_1 - W_0) \times \frac{10,000}{\text{Test Area (cm}^2)}$$

For 40cm² specimens:

$$Cobb_{60} = (W_1 - W_0) \times 250$$

3.3.2. Short-Span Compression Test (SCT)

The Short-Span Compression Test (SCT), depicted in Figure 12, measures edgewise compressive strength of laboratory sheets, indicating containerboard performance in corrugated box manufacturing. To assess METNIN™ SHIELD properties four strips (15-mm wide, ≥8 cm long) are cut from a coated handsheet after measuring and recording grammage. Two strips are conditioned at 23±0.5°C and 50±2% RH, and two at 23±0.5°C and 90±2% RH for at least four hours (overnight preferred).

The test configuration varies by grammage: a 0.7 mm span for samples >80 g/m², and 0.3 mm for <80 g/m², preventing bending before compression. The span-to-thickness ratio must be <5 for valid results, although the thickness does not affect calculations. Grammage is input into the PTA Short-Span Compression Tester to record indexed strength values, enabling comparison across samples [57].

Specimens were removed from the humidity chamber, immediately clamped, and compressed until failure, recording maximum load. A second measurement is taken promptly on the same strip to minimize drying effects, and the procedure was repeated with another strip for four total measurements. The instrument reports the compressive strength (CS) and Compression Index (CI) with deviations [58].

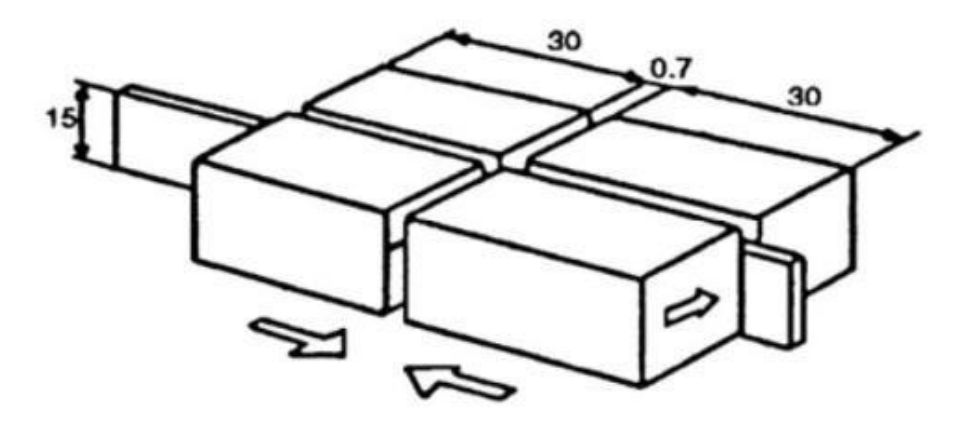
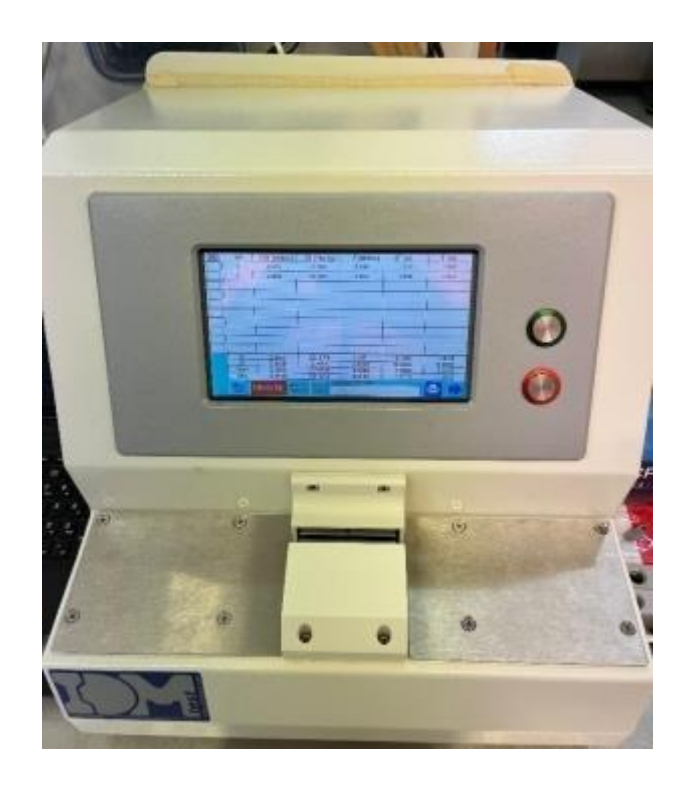


Figure 12: Clamping with 0,7mm free span (TAPPI T 826 om-08)

The CS of containerboards is highly humidity-sensitive, requiring immediate individual testing post-conditioning. To prevent contamination, operators must wear gloves or avoid touching test areas. For statistical validity, the standard deviation of measured values must be ≤10% of the mean; if CI deviation exceeds this, retest at a different strip location.



pic 7, Short span Compression Test compression test

3.4. Integrated Laboratory Process for Handsheet Formation and Semi-Wet Paper Preparation

3.4.1. Raw Material Preparation

The process uses OCC as the primary fiber source, shredded and soaked in water to form a uniform slurry, facilitating fiber separation and pre-swelling. MCC at 15% dry solid content and a 15% METNIN™ SHIELD cover additive enhances structural integrity [59]. MCC integration in Direct addition of MCC into the homogenizer containing the OCC slurry. it has been ensured that homogeneous fiber distribution, with the pulp refining to optimal sheet formation consistency.

Table 3 compares three industrial-scale MCC production methods, highlighting the critical parameters that influence crystallinity and yield.

Material	Dry solid (%)
MCC	15
OCC	92.43
METNIN™ SHIELD	15

Table 3. Dry Solid Content of Materials Used in Composite Formulations.

3.4.3. System Preparation

Preheat the water bath to 92°C–93°C (allow 45 minutes for startup). Ensure the water pressure is between 2.5 and 3 bar, and confirm the circulation pump is operating correctly. Check the forming wire and align the former column. The column is unlocked and opened after formation. A carrier board is placed atop the wet sheet, and excess water is removed by rolling a couching roll perpendicularly twice. The wire was lifted, inverted, and tapped onto a rubber plate to release the sheet, after which it was rinsed and reused [60].

For semi-wet paper two OCC-MCC sheets are layered:

Base layer: Recycled OCC paper.

Core layer: Fresh OCC-MCC slurry.

• **Cover layer:** The final sheet to ensure uniform thickness. The assembly is pressed hydraulically for two minutes to bond layers and remove water.

3.4.4. Drying Procedure

The drying process requires a moisture content below 10%. Sample sheets, placed on carrier boards beside Rapid Köthen (RK) dryers and covered with a non-stick sheet, are dried for seven minutes per sample—optimized for most paper types in the RK system. The procedure includes the following steps:

- 1. Vacuum-assisted drying: The dryer lid was securely closed and the green button maintaining pressure to form a vacuum. Hot water circulation (92–93°C) and vacuum efficiently remove moisture, draining excess through a base coarse screen, enhancing formulation absorption. The vacuum pressure is monitored via a gauge.
- 2. Batch Processing: Dry two samples simultaneously, with a 1-min interval between loadings. An alarm indicates completion; press the button once to stop, holding it to release the residual vacuum.

Laboratory Oven Curing: Conditions: 105°C for one hour (adjustable to simulate pilot-scale mill conditions). Placement: Samples are spaced on shelves to minimize overlap, ensuring even heat distribution.



Pic 8: Oven Curing

3.4.5. Spray coating semi-wet paper sheets

Spray coating semi-wet paper sheets with METNIN™ SHIELD requires optimization of the formulation's viscosity and foaming behavior, which depends on the lignin's source, chemistry, and treatment. Before spraying, the pressure valve and air ventilation system in the spraying cabinet are activated, and the spray gun and its filter are inspected for cleanliness.

Semi-wet sheets are mounted on carrier boards two per test point. The gun, filled with METNIN™ SHIELD, uniformly applied the coating uniformly from 30–40 cm to ensure even distribution and absorption. Deposit assessment relies on visual estimation, posing challenges: insufficient deposition limits strength gains and excess risks leaching. Optimal dry coating deposits range from 5–15 g/m² for most formulations. The coated sheets are then dried and cured. Future work should develop quantitative deposit measurement methods to replace visual estimation [61].

4. Results and discussion

4.1. Calculation of MCC Percentage in Formulations

This research used a water-based gel containing MCC sourced from the Nordic Bioproduct Group, with a dry solid content of 15 wt.% and a neutral pH of 7.

The standard incorporation range for MCC in material formulations typically spans 1%–10% of the total dry weight, ensuring effective integration into the diluted slurry. To calculate the MCC percentage in the mixture, the dry MCC mass was determined from the MCC gel's dry solid content (15 wt.%), and its proportion relative to the total dry fiber mass was computed as follows:

$$MCC\% = \left(\frac{Dry\ MCC\ mass\ (g)}{Total\ dry\ fibers\ (g)}\right) \times 100 = \left(\frac{9550 \times 0.15}{9550}\right) \times 100 = 15\%$$

Processing efficiency:

- **5% MCC:** Direct addition to the slurry is feasible without pre-treatment.
- Above 5% MCC: Pre-dilution in a separate batch using a mechanical mixer is required before homogenization to ensure uniform dispersion.

In METNIN™ SHIELD spray applications, MCC content must not exceed 5% because higher concentrations increase viscosity beyond the operational limits of standard spray guns. A specialized tool with a fine mesh screen was used to ensure an even distribution of the material as a thin, uniform surface layer on the paper substrate.



Pic 9: a water-based gel containing MCC

4.2. Dry Sheet Production and Quality Issues

The dry-sheet production process begins with the initial stages of semi-wet sheet formation. Sheets are formed using a semi-automatic paper-forming machine (Siemens model) and subsequently transferred to an iron drying machine to remove moisture. A SHIELD MetGen coating is then applied through spraying, followed by final drying at 105°C for one hour.

The mechanical strength was evaluated using an IDM Short-Span Compression Tester (SCT07), measuring the following key parameters:

- 1. **Compression Strength (CS):** Absolute compressive resistance, measured in kN/m.
- 2. Compression Index (CI): Normalized strength relative to density, expressed in Nm/g.
- 3. **CS/Grammage Ratio:** Strength-to-weight relationship, reported in kN·m/g [62].

Grammage-normalized CS values facilitated direct comparisons across sheets with varying basis weights, while CI measurements assessed intrinsic material properties independent of density. This testing protocol systematically evaluated the reinforcing effects of MCC across a concentration gradient.

However, the method exhibited the following quality issues:

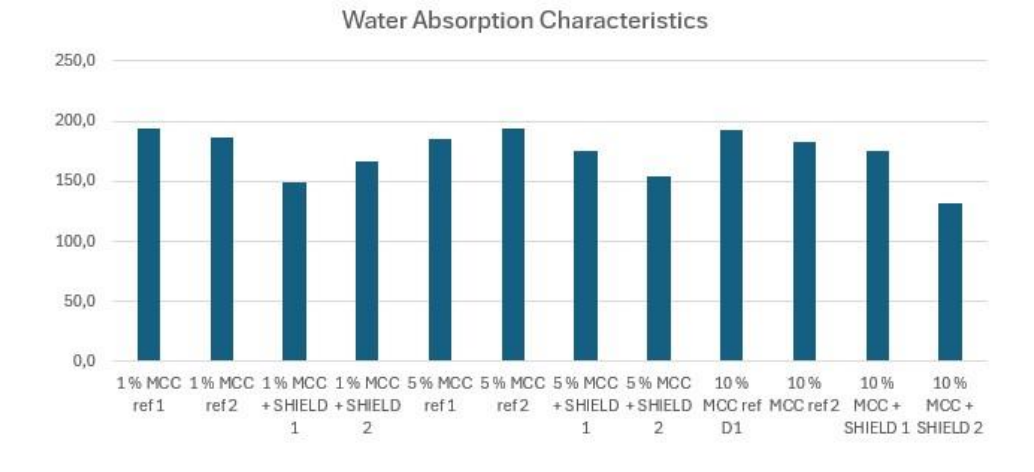
- 1. Brown-colored print leaching remained visible, failing to meet industry standards.
- 2. Water absorption performance was inadequate during testing.
- 3. Strength test results were marginally acceptable, falling within the mid-range of industry standards.

60	dry	wet	Wow	Leaching	Grammag	Average grammage	Deposit	CS	C\$±	CI	CI±	Impr. 50 %	CS	C5±	CI	CI±	Impr. 90 %
10 % MCC ref DI	0,542	1,314	193,0	yes	97,8	97,8		2,151	0,152	21,993	1,553	3	1,441	0,146	14,73	1,497	
10 % MCC ref 2	0,542	1,271	182,3	yes	97,8												
10 % MCC + SHIELD 1	0,602	1,305	175,8	yes	108,7	108,8	11,0	2,455	0,091	22,565	0,839	2,6	1,598	0,065	14,688	0,601	-0,3
10 % MCC + SHIELD 2	0,604	1,131	131.8	yes	109,0			-171		1 1				100	1 - 1	5 "	
1 % MCC ref 1	0,536	1,314	194,5	yes.	96,7	97,5		2,249	0,055	22,479	1,494		1,456	0,058	14,931	0,599	
1 % MCC ref 2	0,544	1,289	186,3	yes	98,2		1	92000						2 88000	-		
1 % MCC + SHIELD 1	0,598	1,194	149,0	yes	107,9	106.9	9,5	4,075	0,158	19,909	1,052	77,5	1,656	0,091	15,495	0,856	2,8
1 % MCC + SHIELD 2	0,587	1,254	166,8	yes	106,0	10.000											
5 % MCC ref 1	0,54	1,281	185,3	yes	97,5	97,7		2,317	0,017	23,711	0,171		1,466	0,122	14,675	1,331	- 3
5 % MCC ref 2	0,543	1,321	194,5	yes	98,0												
5 % MCC + SHIELD 1	0,61	1,313	175,8	yes	110,1	110,6	12,9	2,544	0,212	23,006	1,916	-3,0	1,574	0,102	15,134	0,923	3,1
5 % MCC + SHIELD 2	0,616	1,233	154,3	yes	111,2												

Table 4, MCC test results for cobb & sct



pic 10: cobb test of the dry sheet



pic 11: Water Absorption Characteristics dry sheet

4.3. Semi-Wet Application and Mechanical Testing

This experimental process utilized semi-wet paper sheets to assess material performance in multiple test configurations. Sheets with MCC concentrations ranging from 1% to 10%, alongside control samples with no MCC were examined for comparative analysis.

- **5% MCC:** Highest water resistance (Cobb60 = 68.8 g/m² vs. 202 g/m² for control).
- **10% MCC:** Peak compressive strength (CS=3.6 kN/m), though spray ability was reduced due to increased viscosity.



Table 5: result of test of MCC for cobb & sct percentages (1-10%)

4.3.1. Properties of MCC Incorporation Semi-Wet Paper Sheets

The findings suggest that MCC incorporation improves water resistance without leaching risks, with the 5% concentration offering an optimal balance of performance and material economy. A concentration-dependent relationship was observed between MCC content and compressive strength, with progressive increases (1% to 10%) enhancing structural integrity, peaking at 10% (CS=3.6 kN/m). However, other strength properties remained comparable across concentrations.

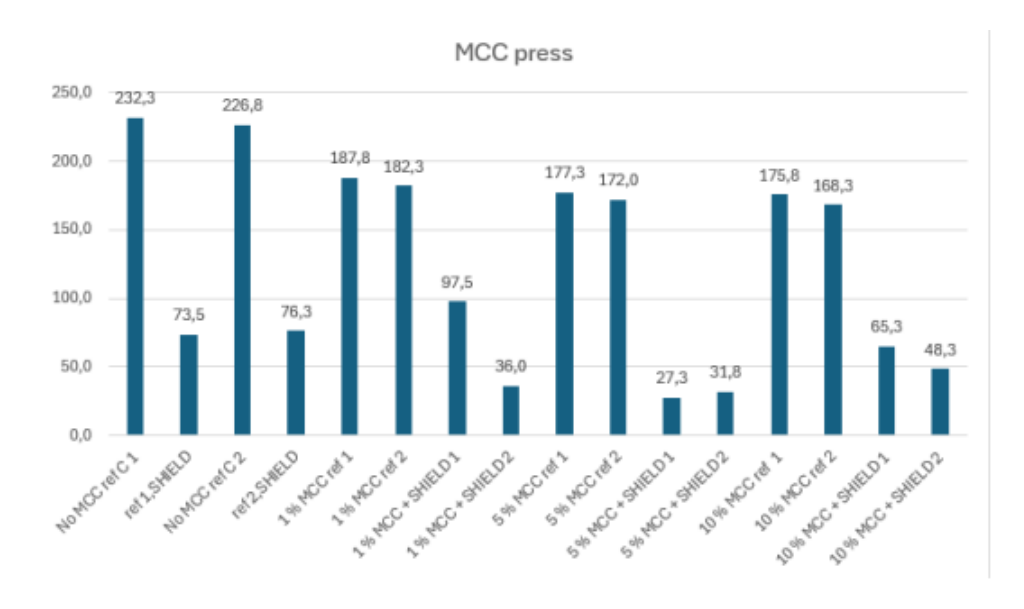


Figure 13: Water Absorption Characteristics of Semi-Wet Paper Sheets with Varying MCC Concentrations.

The water absorption results cut straight to the point and outline water resistance capabilities; absorption values lower than 27 g/m² are categorized as "very good" and are considered exceptional. Additional notable conclusions are as follows:

- Optimal Conditions: The best results, close to or surpassing the benchmark, were recorded with 5% MCC and SHIELD D2 (27.3 g/m²) and with 10% MCC and SHIELD D1 (31.8 g/m²) for water resistance. This implies that moderate MCC concentrations result in extreme treatment results when incorporated with SHIELD.
- Challenges at Higher Concentrations: The 10% MCC + SHIELD D2 samples depict mixed trends; some values such as 175.8 and 168.3 g/m² are exceptionally low outliers. This degree of variability may point to difficulties with the treatment application or sample preparation at greater MCC concentrations, therefore more analysis is required.

This study evaluated SHIELD-MCC formulations applied to semi-wet OCC sheets in two phases. Initially, increasing the MCC content raised formulation viscosity, rendering spray application impractical beyond 5%, necessitating manual coating for higher concentrations.

Subsequent testing showed that lower MCC concentrations (e.g., 1%) optimized functional performance, Mechanical testing indicated comparable strength across all tested concentrations (1%, 5%, and 10%), suggesting that MCC's influence on mechanical properties is limited within this range. Thus, the 1% formulation emerges as the optimal balance of performance and process efficiency.

MCC	Processability	CapillaryRise	Water	Strength
Concentration (%)		(CP)	Resistance	Performance
1	Excellent (sprayable)	Highest	Best	Medium range
5	Moderate	Moderate	Good	Medium range
10	Poor (manual only)	Lowest	Fair	Medium range

Table 6: Evaluation of MCC Performance Across Key Sheet Properties.

4.3.2. Properties of MFC on Semi-Wet Paper Sheets

This section investigates the performance of MFC in semiwet paper sheets across various concentrations. Experimental results revealed concentration-dependent effects. At 1% concentration, MFC exhibited optimal water resistance, as indicated by the highest capillary rise (CP) values. This suggests that lower concentrations enhance functional properties effectively. However, mechanical strength remained consistent across the tested range (1%, 5%, and 10%), indicating no significant structural variation with MFC content.

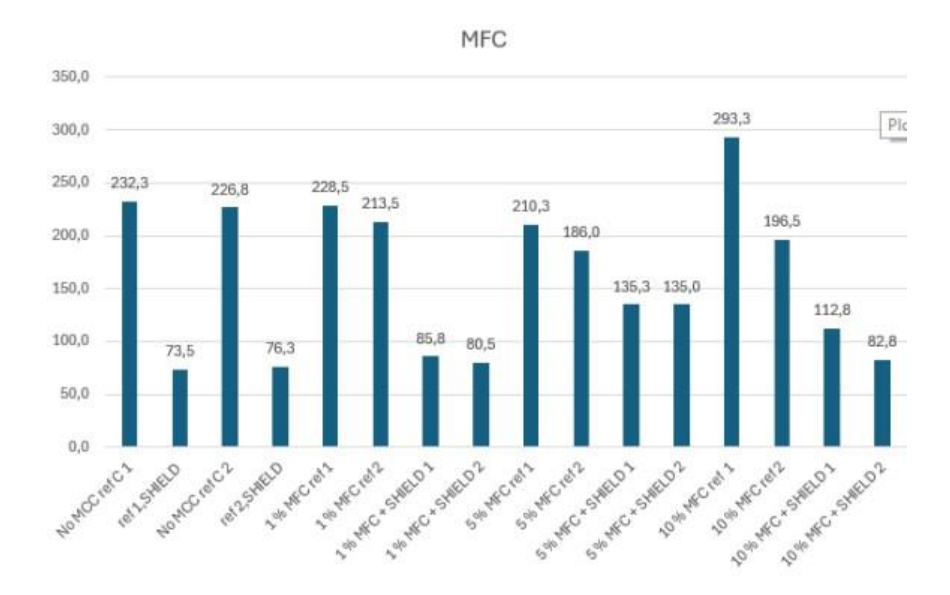


Figure 14: Water Absorption Rates of MFC Composites at Concentrations from 1% to 10%.

4.4. SEM characterization

Scanning electron microscopy (SEM) analysis was conducted to examine the microstructural effects of MCC on composite sheets. Figure 15 illustrates the shape and surface morphology of MCC, revealing a flake-like structure with irregular dimensions [63]. The influence of MCC on the fracture surface morphology of rHDPE/cantala fiber composites is shown in Figure 16: SEM Images of Fracture Surfaces Showing Void Reduction with 4% MCC.

These images confirm MCC's role in reducing voids: at 0% MCC, fiber pullouts indicate poor fiber-matrix adhesion, whereas at 4% MCC, a dense matrix (arrows in Figure 16e) reflects improved bonding [64].

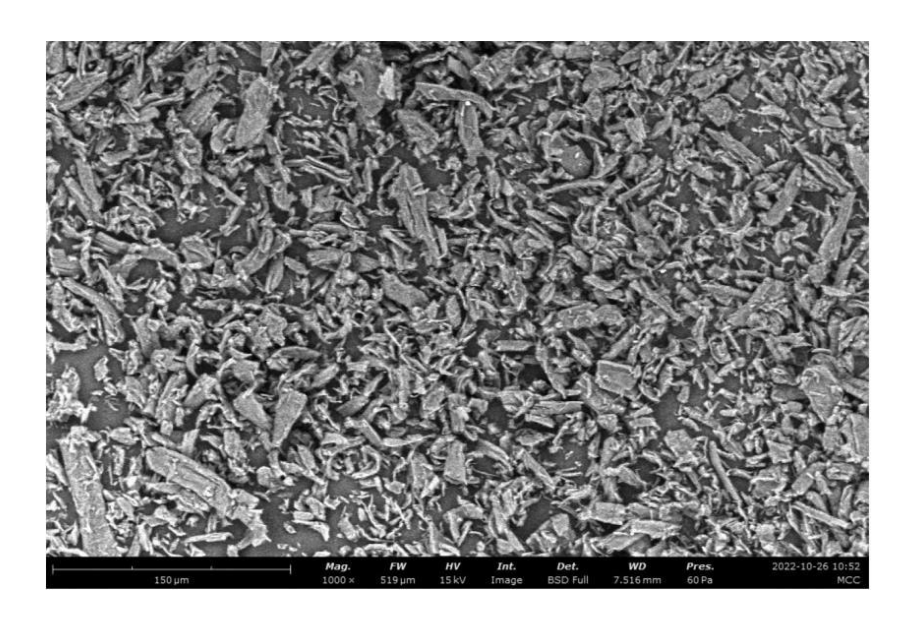


Figure 15. SEM image of MCC, Scale bars: 10 µm [64].

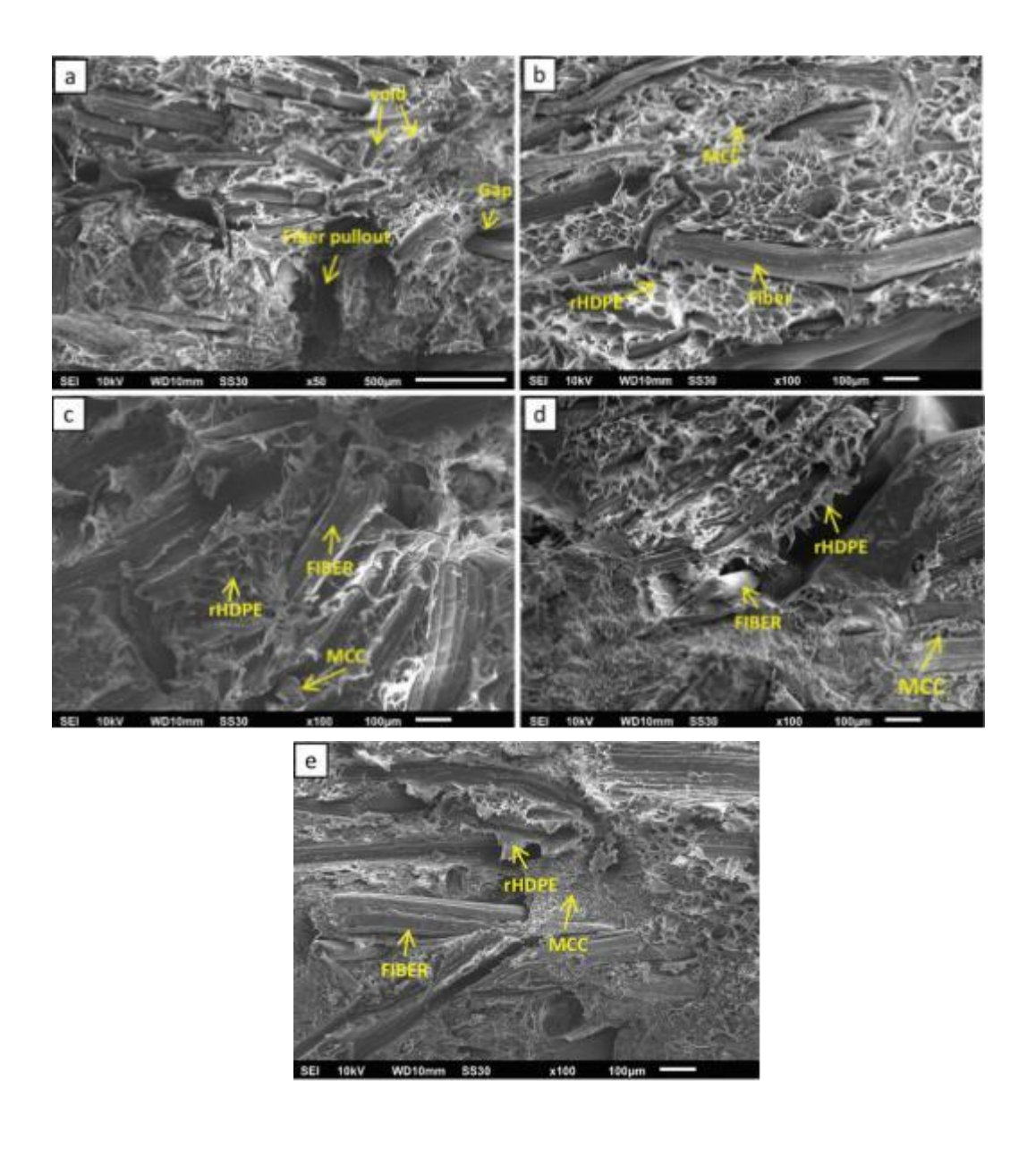


Figure 16. SEM micrograph of composite tensile fracture surface with MCC: (a) 0% wt; (b)1%wt; (c) 2%wt; (d) 3%wt; (e) 4%wt. [64]

4.5. FTIR Characterization

Fourier Transform Infrared (FTIR) spectroscopy analysis elucidated key structural features of recycled high-density polyethylene (rHDPE)/cantala fiber composites, both with and without MCC incorporation [65]. The FTIR spectrum of pure rHDPE exhibited characteristic absorption bands at 2923 cm⁻¹ (asymmetric C-H stretching), 1475 cm⁻¹ (CH₃ bending), and 717-730 cm⁻¹ (CH₂ rocking), which are consistent with its hydrocarbon composition [66].

Cantala fiber displayed distinct peaks at 3400 cm⁻¹ (O-H stretching of hydroxyl groups), 2850 cm⁻¹ (symmetric CH₂ stretching), and 1732 cm⁻¹ (C=O stretching of hemicellulose carbonyl groups). [66] The MCC spectrum showed similarities to that of cantala fiber but featured additional peaks at 2900 cm⁻¹ (C-H stretching), 1374 cm⁻¹ (C-H bending), 1035-1060 cm⁻¹ (C-O stretching in cellulose), and 890 cm⁻¹ (glycosidic linkages), indicative of its crystalline cellulose structure. The incorporation of MCC induced several significant spectral changes [66]. Most notably, the O-H stretching region around 3240 cm⁻¹ exhibited broadening and increased intensity, suggesting enhanced hydrogen bonding between the hydroxyl groups of MCC and the rHDPE matrix. Simultaneously, the intensity of the hemicellulose-associated C=O stretching peak at 1740 cm⁻¹ diminished, indicating the partial removal of amorphous hemicellulose components [67].

A comparable reduction was observed in the lignin-related C-O peak at 1240 cm⁻¹. These spectral modifications demonstrate that MCC addition facilitates two key structural enhancements: (1) improved interfacial adhesion through hydrogen bond formation and (2) increased overall crystallinity by reducing the content of amorphous hemicellulose and lignin.

These structural improvements directly correspond to the enhanced mechanical properties observed in the composites. The stronger interfacial bonding and elevated crystallinity enable more efficient stress transfer within material [68].

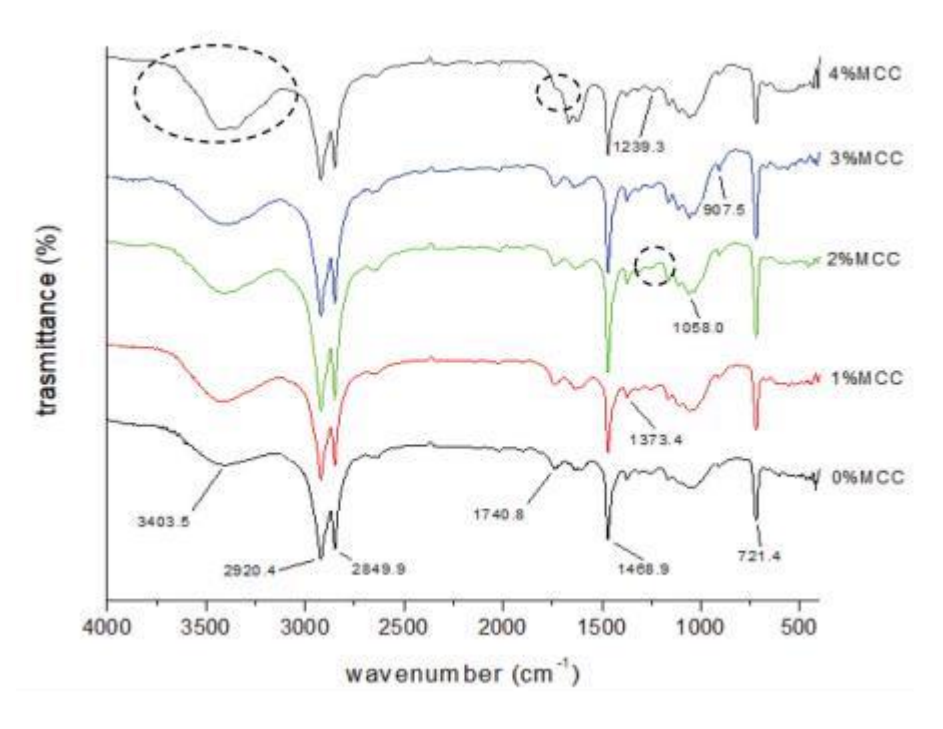


Figure 17. FTIR spectra of cantala/rHDPE composites with varying MCC concentrations

Table 1. Peak FTIR spectrum of the cantala/rHDPE/MCC composite.

Wavenumber (Vavenumber (cm ⁻¹)					
0% MCC	1% MCC	2% MCC	3% MCC	4% MCC	Functional Group	
721.41	720.44	721.41	721.41	719.48	C-C Stretch	
1056.07	1057.04	1058.00	1058.00	1058.00	C-O Stretch	
1468.86	1467.89	1468.86	1468.86	1468.86	C-H Bend	
1636.67	1604.84	1637.64	1640.53	1621.24	C=C Stretch	
1740.83	1738.90	1737.94	1737.94	1665.60	C=O Stretch	
2849.95	2849.95	2849.95	2849.95	2849.95	C-H Stretch	
2919.39	2919.39	2919.39	2919.39	2920.35	C-H Stretch	
3374.61	3386.18	3398.72	3421.87	3427.65	O-H Stretch	

Table 1: FTIR peak assignments for cantala/rHDPE/MCC composites at different MCC concentrations [68].

4.6. XRD characterization

Figures 18 and 19 illustrate the X-ray diffraction (XRD) patterns of rHDPE, MCC, and their composite materials. The XRD pattern of MCC exhibits characteristic peaks at 15.6° (110 plane, amorphous region), 22.96° (200 plane, crystalline region), and 34.72° (004 plane, amorphous region), with the prominent 22.96° peak confirming cellulose Iβ crystallinity [69]. The rHDPE matrix displays peaks at 21.62° and 23.92°, corresponding to the (110) and (200) planes, respectively, which are retained in the composites. Figure 19 provides a detailed comparison of the XRD patterns for rHDPE, MCC, and the composites, accompanied by crystallographic data [70].

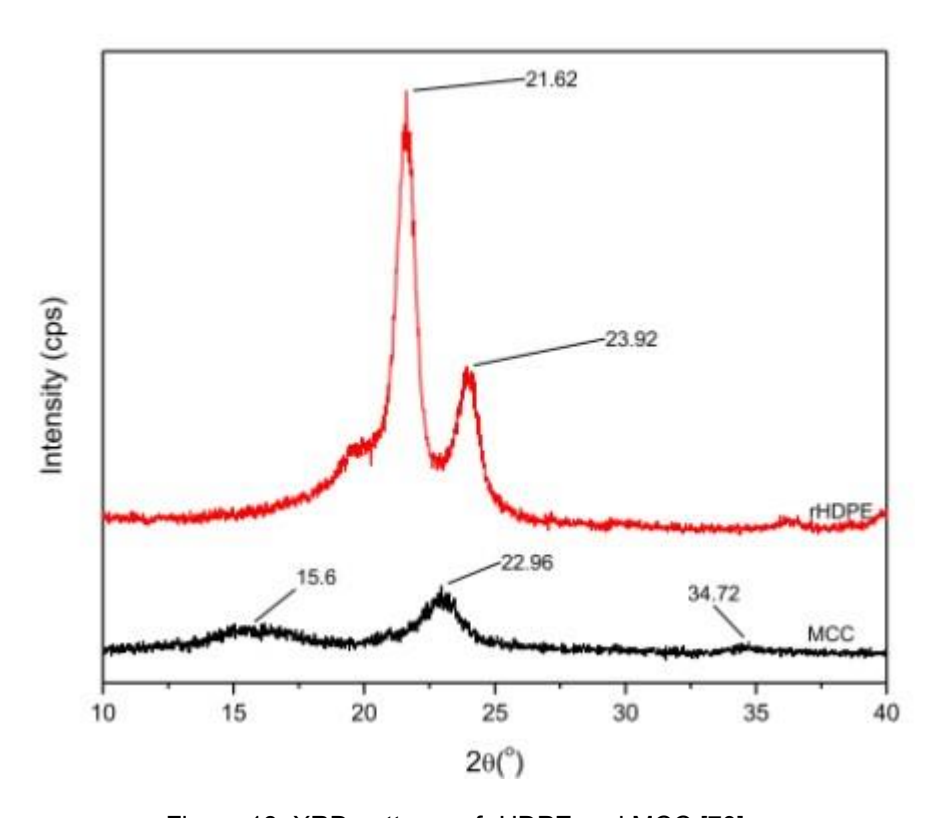


Figure 18. XRD patterns of rHDPE and MCC [70].

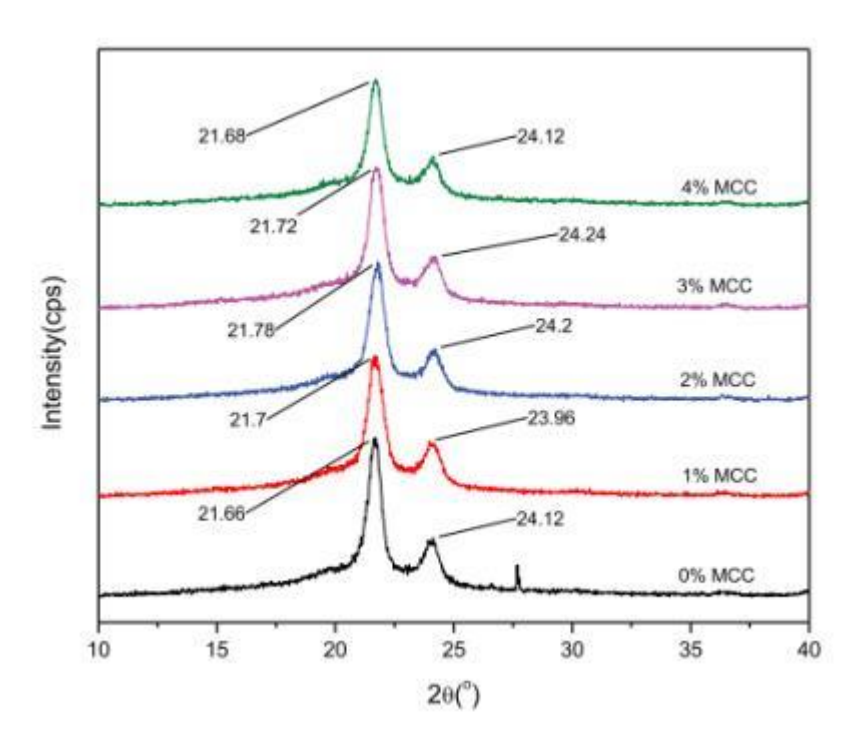


Figure 19. XRD patterns of rHDPE, MCC, and cantala/rHDPE composites with varying MCC concentrations, including crystallographic data [70].

Table 2. The crystallinity of cantala fiber/rHDPE composites with variations in MCC weight fraction.

	Peak Pos	ition (2θ)	Crystallinity Index (%)		
Composites	(110)	(200)			
rHDPE/cantala/0%MCC	21.66	24.12	48.02		
rHDPE/cantala/196MCC	21.70	23.96	49.09		
rHDPE/cantala/2%MCC	21.78	24.20	49.87		
rHDPE/cantala/3%MCC	21.72	24.24	50.90		
rHDPE/cantala/4%MCC	21.68	24.12	51.45		

Table 2. Crystallinity indices of cantala fiber/rHDPE composites with different MCC weight fractions [70].

Notably, while MCC incorporation did not induce peak shifting, it significantly enhanced the composite's crystallinity. The crystallinity index increased by 6.7% (from 48.02% to 51.45%) with four wt% MCC addition, accompanied by a 22% increase in peak intensity at approximately 22°. This crystallinity enhancement can be attributed to two factors: (1) the intrinsic crystallinity of MCC itself, and (2) nucleation effects promoting rHDPE matrix crystallization [71].

These structural modifications are directly correlated with improved mechanical performance. Also increased *The bending strength improved The bending strength improved* enhances tensile strength, modulus of elasticity, and ductility through several mechanisms:

- 1. Improved stress transfer via more ordered crystalline regions
- 2. Reduced molecular chain mobility in crystalline phases
- 3. Enhanced interfacial adhesion between matrix and reinforcement

The optimal crystallinity achieved at 4 wt% MCC loading demonstrates the effectiveness of cellulose crystals as both reinforcing fillers and crystallization promoters in recycled polymer systems [72].

4.8. Density Properties

The density variations in MCC-reinforced composites are visualized through Figure 21 which displays values between 0.88 g/cm³ and 0.90 g/cm³. The gradual density increases with MCC loading demonstrates the filler's effectiveness in reducing composite porosity [73]. This enhancement occurs through two primary mechanisms: MCC particles physically filling the interfacial voids between fibers and matrix, and improved polymer-fiber adhesion leading to better structural consolidation. The resulting denser composite morphology contributes to both improved physical properties and mechanical performance [74].

4.8.1. Tensile Properties

The tensile strength evolution shown in Figure 21 highlights MCC's reinforcing capability. Starting from a baseline value of 29.10 MPa for the unreinforced composite, systematic increases were observed with MCC addition up to four wt% [75]. This strengthening effect originates from the combined action of several factors: enhanced stress transfer through improved interfacial adhesion (per SEM observations), increased matrix crystallinity (6.7% rise from XRD data), and more efficient load distribution due to reduced void content [76] [75]. These mechanical property improvements confirm that MCC successfully modifies the composite at multiple structural levels, from molecular interactions to macroscopic performance.

The composite reinforced with 4 wt% MCC demonstrated optimal tensile performance, achieving a maximum strength of 43.85 MPa. This represents a significant 50.7% improvement over the unreinforced composite (29.10 MPa) [77]. The substantial enhancement stems from MCC's multifunctional role during composite processing and loading. During melt mixing in the twin-screw extruder, MCC particles become uniformly dispersed and form strong interfacial bonds with the rHDPE matrix. These bonded MCC particles subsequently fill the inter-fiber voids and pores, creating a more continuous and cohesive material structure [78].

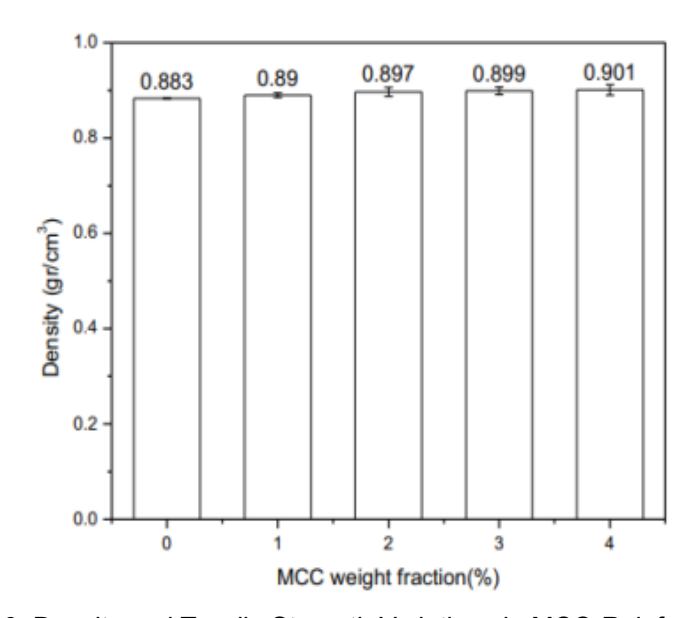


Figure 20. Density and Tensile Strength Variations in MCC-Reinforced Composites [78].

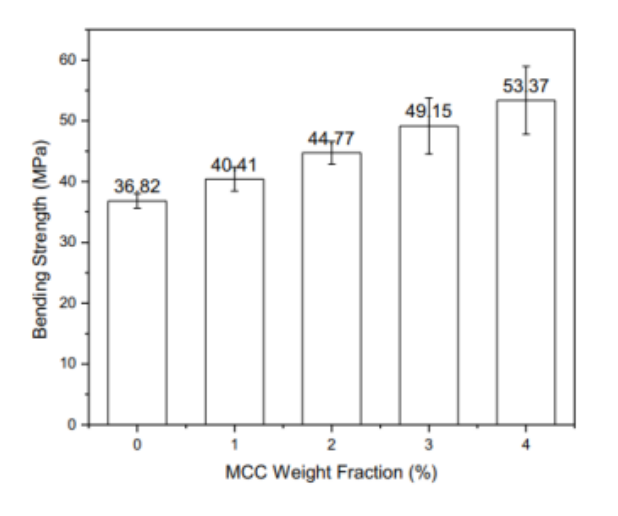
4.9. Bending Strength Properties

demonstrates the impact of MCC on the bending strength of cantala fiber/ rHDPE composites. The research shows a substantial strength improvement in flexural properties after MCC introduction with the composite consisting of four percent MCC reaching a peak strength of 53.37 MPa. The composite with MCC content reached a flexural strength of 53.37 MPa which exceeded the base compound strength of 40.74 MPa by 31% according to the reported percentage improvement [79].

The increased strength of the material results from the following three fundamental factors including (1) proper MCC arrangement in rHDPE material (2) strong interfacial connections between composite elements and (3) effective MCC particle distribution in void spaces among cantala fibers. The study shows that the 31% strength improvement in the 4 wt% MCC loading matches with increased crystallinity index revealed through XRD analysis (48.02% to 51.45%) and decreased void content as shown in SEM micrographs [80].

Figure 21 illustrates that the bending modulus strengthens at the same rate as the reinforcement process. The material containing 4 wt% MCC achieves a bending modulus of 1.96 GPa which surpasses the 1.1 GPa performance of the control composite with 0 wt% MCC. The mechanical strength enhancement results primarily from the combination of MCC stiffness with its capacity to establish an extensive matrix-reinforcement interface. The uniform MCC particle distribution in the composite structure improves stress transfer through the matrix while preventing deformation of the material [81] [80].

The composite material demonstrates improved load-bearing capability together with enhanced deformation resistance through the reinforcement effect of MCC. The modified composition makes the material a suitable choice for structures that need to maintain their original dimensions when exposed to mechanical loads [82].



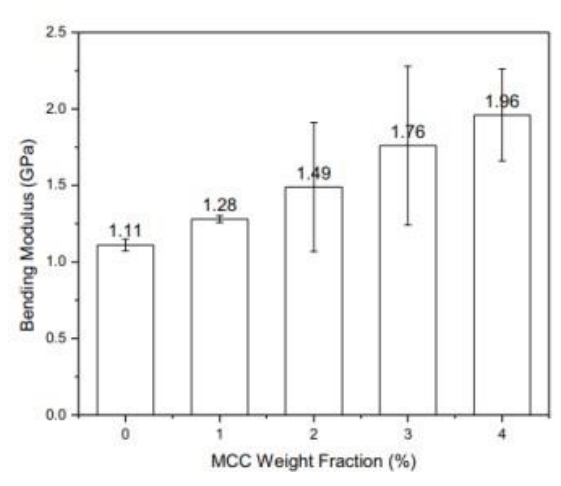


Figure 21. Bending Strength of MCC-Reinforced rHDPE/Cantala Composites [82].

5. Conclusion

In this study, we examined different concentrations of MCC in OCC composites to optimize spray-coating performance. Systematic testing and analysis revealed that 4 wt% MCC delivers the best overall balance: it significantly boosts strength and water resistance while keeping the mixture fluid enough for spraying. For example, increasing MCC to 10 wt% raised the composite's compressive strength to about 3.6 kN/m (versus ~2.8 kN/m for the uncoated OCC), but the formulation became so viscous that it could not be spray-applied beyond roughly 5 wt%. In contrast, at 4 wt% the formulation remained fluid enough to spray and still provided substantial performance gains.

Specifically, the 4 wt% composite exhibited markedly improved water resistance (lower Cobb60 values and reduced capillary rise), achieving a water-barrier performance comparable to the 5 wt% coating but without any processing drawbacks. Its compressive strength was essentially on par with that of higher-concentration blends, suggesting that adding more MCC beyond this point yields diminishing returns. Overall, these findings indicate that using 4 wt% MCC offers the optimal compromise between ease of processing and enhanced composite performance.

5.1. Implications and Benefits

Our results suggest that using just 4 wt% MCC strikes a great balance between sustainability and performance. Since the base sheets are made from OCC, adding only a small amount of MCC drastically cuts down on raw material use while still meeting strength and water-resistance targets. In practice, this resource-efficient approach means clear environmental advantages and cost savings: we lower material expenses without sacrificing quality. We also found that the 4 wt% formula sprays very easily, which is a big practical win. Spray coating remains a fast, flexible method at this concentration, allowing a plant to coat large areas quickly with standard equipment. At the same time, the resulting coating makes the material tougher: it boosts water resistance and compressive strength, helping protect packages from moisture and handling stresses. In short, this "sweet spot" formulation delivers most of the benefits of higher cellulose content (like better barrier performance and durability) without the processing drawbacks, offering both environmental and economic gains.

5.2. Limitations and Future Directions

There are a few limitations that we need to keep in mind. For example, we estimated coating thickness by eye, which can be subjective and may vary between different observers. In future work, it would be better to use quantitative methods – such as gravimetric or spectroscopic techniques – to measure coating thickness and uniformity precisely. Objective measurements like these would improve precision and reproducibility, which is crucial for validating the process in an industrial setting. Another limitation is that all our testing was done at the lab scale. Scaling up to a real factory brings its own challenges. We will need fine-tune spray parameters (nozzle design, pressure, flow rate, etc.) for industrial equipment, and carefully evaluate costs and performance in real-world conditions. In this context, conducting pilot-scale trials will be especially important. Pilot testing can show how the coating behaves in a production environment and help uncover any unexpected issues before moving to full-scale manufacturing.

6. References

- 1. Abatzoglou, N., Chornet, E., Belkacemi, K. & Overend, R.P., Phenomenological kinetics of complex systems: the development of a generalized severity parameter and its application to lignocellulosics fractionation, Chem. Eng. Sci. 47 (1992) no. 5 pp. 1109–1122.
- 2. Andersson, S., Wikberg, H., Pesonen, E., Maunu, S.L. & Serimaa, R., Studies of crystallinity of Scots pine and Norway spruce cellulose, Trees 18 (2004) no. 3 pp. 346–353.
- 3. Avicel, Avicel,
- http://www.fmcbiopolymer.com/Pharmaceutical/Products/Avicelforsoliddoseforms.aspx, accessed 20.8.2016 (2016).
- 4. Girisuta, B., Janssen L. P. B. M. & Heeres H. J., Kinetic Study on the Acid-Catalyzed Hydrolysis of Cellulose to Levulinic Acid, Ind. Eng. Chem. Res. 46 (2007) no. 6 pp. 1696–1708.
- 5. Baktash, M.M., Ahsan, L. & Ni, Y., Production of furfural from an industrial pre-hydrolysis liquor, Sep. Purif. Technol. 149 (2015) pp. 407–412.
- Battista, O.A., Food compositions incorporating cellulose crystallite aggregates, (1962)
 US3023104 A.
- 7. Battista, O.A. & Smith, P.A., Level-off d.p. cellulose products, (1961) US2978446 A.
- 8. Battista, O.A., Coppick, S., Howsmon, J.A., Morehead, F.F. & Sisson, W.A., Level-Off Degree of Polymerization, Ind. Eng. Chem. 48 (1956) no. 2 pp. 333–335.
- Battista, O.A., Hydrolysis and crystallization of cellulose, Ind. Eng. Chem. 42 (1950) no. 3 pp.

502-507.

- Baugh, K.D. & McCarty, P.L., Thermochemical pretreatment of lignocellulose to enhance methane fermentation: I. Monosaccharide and furfurals hydrothermal decomposition and product formation rates, Biotechnol. Bioeng, 31 (1988) no. 1 pp. 50–61.
- 11. Berg J.M., Tymoczko J.L. & Stryer L., Section 11.2, Complex Carbohydrates Are Formed by Linkage of Monosaccharides, Biochemistry 5th edition (2002) New York W.H. Freeman.
- 12. Bozell, J.J., Moens, L., Elliott, D.C., Wang, Y., Neuenschwander, G.G., Fitzpatrick, S.W., Bilski, R.J. & Jarnefeld, J.L., Production of levulinic acid and use as a platform chemical for derived products, Resour. Conserv. Recy. 28 (2000) no. 3–4 pp. 227–239.
- 13. Brasch, D. & Free, K., Prehydrolysis-kraft pulping of Pinus radiata grown in New Zealand, Tappi 48 (1965) no. 4 pp. 245–248.

- 14. Brinchi, L., Cotana, F., Fortunati, E. & Kenny, J.M., Production of nanocrystalline cellulose from lignocellulosic biomass: Technology and applications, Carbohydr. Polym. 94 (2013) no. 1 pp. 154–169.
- 15. Chaplin, Water structure and science, http://www1.lsbu.ac.uk/water/cellulose.html, accessed 29.07.2016.
- 16. Chinga-Carrasco, G., Cellulose fibres, nanofibrils and microfibrils: The morphological sequence of MFC components from a plant physiology and fibre technology point of view, Nanoscale Res. Lett. 6 (2011) no. 1 pp. 417.
- 17. Chum, H.L., Johnson, D.K., Black, S.K. & Overend, R.P., Pretreatment-Catalyst effects and the combined severity parameter, Appl. Biochem. Biotechnol. 24 (1990) no. 1 pp. 1–14.
- Ciolacu, D. & Popa, V.I., Cellulose allomorphs: Structure, accessibility and reactivity, 1st edition (2010), Polymer Science and Technology Series, Nova Science Publisher, Inc. New York, 70 pp. ISBN 978-1-61668-323-8.
- 19. Ding, S., Zhao, S. & Zeng, Y., Size, shape, and arrangement of native cellulose fibrils in maize cell walls, Cellulose 21 (2014) no. 2 pp. 863–871.
- 20. Krueger, C., Thommes, M. & Kleinebudde, P., Influence of MCC II fraction and storage conditions on pellet properties, Eur. J. Pharm. Biopharm. 85 (2013) no. 3, Part B, pp. 1039–1045.
- 21. Kupiainen, L., Dilute acid catalysed hydrolysis of cellulose Extension to formic acid, Dissertation, University of Oulu, Faculty of Technology, Department of Process and Environmental Engineering, Chemical Process Engineering Laboratory, Oulu (2012) pp. 65.
- 22. Laka, M., & Chernyavskaya, S., Obtaining of microcrystalline cellulose from softwood and hardwood pulp, BioResources 2 (2007) no. 4.
- 23. Leppänen, K., Andersson, S., Torkkeli, M., Knaapila, M., Kotelnikova, N. & Serimaa, R., Structure of cellulose and microcrystalline cellulose from various wood species, cotton and flax studied by X-ray scattering", Cellulose, 16 (2009) no. 6 pp. 999–1015.
- 24. Li, J., Wang, L. & Chen, H., Periodic peristalsis increasing acetone–butanol–ethanol productivity during simultaneous saccharification and fermentation of steam-exploded corn straw, J. Biosci. Bioeng. (2016) pp. 1389–1723.
- 25. Liitiä, T., Maunu, S.L., Hortling, B., Tamminen, T., Pekkala, O. & Varhimo, A., Cellulose crystallinity and ordering of hemicelluloses in pine and birch pulps as revealed by solid-state NMR spectroscopic methods, Cellulose, 10 (2003) no. 4 pp. 307–316.

- 26. Lin, N. & Dufresne, A., Nanocellulose in biomedicine: Current status and future prospect, Eur. Pol. J. 59 (2014) pp. 302–325.
- 27. Liu, X., Xu, Q., Liu, J., Yin, D., Su, S. & Ding, H., Hydrolysis of cellulose into reducing sugars in ionic liquids, Fuel 164 (2016) pp. 46–50.
- 28. Lloyd, J.A. & Horne, C.W., The determination of fibre charge and acidic groups of radiata pine pulps, Nord. Pulp. Pap. Res. J. 8 (1993) no. 1 pp. 48–52.
- 29. Lu, Y. & Mosier, N.S., Kinetic modeling analysis of maleic acid-catalyzed hemicellulose hydrolysis in corn stover, Biotechnol. Bioeng. 101 (2008) no. 6 pp. 1170–1181.
- 30. Mansikkamäki, P., Lahtinen, M. & Rissanen, K., The conversion from cellulose I to cellulose II in NaOH mercerization performed in alcohol–water systems: An X-ray powder diffraction study, Carbohydr. Polym. vol. 68 (2007) no. 1 pp. 35–43.
- 31. Matthews, J., Himmel, M. & Crowley, M., Conversion of cellulose Iα to Iβ via a hightemperature intermediate (I-HT) and other cellulose phase transformations, Cellulose 19 (2012) no. 1 pp. 297–306.
- 32. Moon, R.J., Martini, A., Nairn, J., Simonsen, J. & Youngblood, J., Cellulose nanomaterials review: structure, properties and nanocomposites, Chem. Soc. Rev. 40 (2011) no. 7 pp. 3941–3994.
- 33. Mu, B., Xu, H. & Yang, Y., Accelerated hydrolysis of substituted cellulose for potential biofuel production: Kinetic study and modeling, Bioresour. Technol. 196 (2015) pp. 332–338.
- 34. Mukherjee, A., Dumont, M. & Raghavan, V., Review: Sustainable production of hydroxymethylfurfural and levulinic acid: Challenges and opportunities, Biomass Bioenergy 72 (2015) pp. 143–183.
- 35. Palme, A., Theliander, H. & Brelid, H., Acid hydrolysis of cellulosic fibres: Comparison of bleached kraft pulp, dissolving pulps and cotton textile cellulose, Carbohydr. Polym. 136 (2016) pp. 1281–1287.
- 36. Parveen, F., Patra, T. & Upadhyayula, S., Hydrolysis of microcrystalline cellulose using functionalized Bronsted acidic ionic liquids A comparative study, Carbohydr. Polym. 135 (2016) pp. 280–284.
- 37. Peleteiro, S., Rivas, S., Alonso, J.L., Santos, V. & Parajó, J.C., Furfural production using ionic liquids: A review, Bioresour. Technol. 202 (2016) pp. 181–191.
- 38. Peng, B.L., Dhar, N., Liu, H.L. & Tam, K.C., Chemistry and applications of nanocrystalline cellulose and its derivatives: A nanotechnology perspective, Can. J. Chem. Eng. 89 (2011) no. 5 pp. 1191–1206.

- 39. Qi, B., Luo, J., Chen, G., Chen, X. & Wan, Y., Application of ultrafiltration and nanofiltration for recycling cellulase and concentrating glucose from enzymatic hydrolyzate of steam-exploded wheat straw, Bioresour. Technol. 104 (2012) pp. 466–472.
- 40. Rajalaxmi, D., Jiang, N., Leslie, G. & Ragauskas, A.J., Synthesis of novel water-soluble sulfonated cellulose, Carbohydr. Res. 345 (2010) no. 2 pp. 284–290.
- 41. Rocha, G.J.M., Gonçalves, A.R., Nakanishi, S.C., Nascimento, V.M. & Silva, V.F.N., Pilot scale steam explosion and diluted sulfuric acid pretreatments: Comparative study aiming the sugarcane bagasse saccharification, Ind. Crops Prod. 74 (2015) pp. 810–816. 42. Rojas, J., Effect of Polymorphism on the Particle and Compaction Properties of Microcrystalline Cellulose, Cellulose Medical, Pharmaceutical and Electronic Applications (2013) Theo van de Ven & Louis Godbout (Ed.), InTech, DOI: 10.5772/56591.
- 43. Saeed, A., Jahan, M.S., Li, H., Liu, Z., Ni, Y. & van Heiningen, A., Mass balances of components dissolved in the pre-hydrolysis liquor of kraft-based dissolving pulp production process from Canadian hardwoods, Biomass Bioenergy 39 (2012) pp. 14–19. 44. Saeman, J.F., Kinetics of Wood Saccharification Hydrolysis of Cellulose and Decomposition of Sugars in Dilute Acid at High Temperature, Ind. Eng. Chem. 37 (1945) no. 1 pp. 43–52.
- 45. SCAN CM 65:02, SCAN –test standards: Pulp Total acidic group content Conductometric titration method, Stockholm: Scandinavian Pulp, Paper, and Board testing committee, (2002).
- 46. SCAN C 15:99, SCAN –test standards: Pulp Viscosity in cupriethylenediamine (CED) solution, Stockholm: Scandinavian Pulp, Paper, and Board testing committee, (1999).
- 47. SCAN 15:88, SCAN –test standards: Pulp Viscosity in cupriethylenediamine (CED) solution, Stockholm: Scandinavian Pulp, Paper, and Board testing committee, (1988).
- 48. SCAN C 03:78, SCAN –test standards: Pulps determination of dry matter content, Stockholm: Scandinavian Pulp, Paper, and Board testing committee, (1978).
- 49. Dufresne, A., Nanocellulose: From Nature to High Performance Tailored Materials, (2012) Boston, De Gruyter, pp. 460. Retrieved 6 Sep. 2016, from [http://www.degruyter.com/view/product/129215](http://www.degruyter.com/view/product/12921) 50. Boeva, R & Spiridonov I 2015, 'Types of fibrous materials used in the pulp and paper industry and their leaf-forming properties', Scientific papers of the University of Jirus, vol. 54, pp. 112-116.
- 51. Asim, M, Abdan, K, Jawaid, M, Nasir, M, Dashtizadeh, Z, Ishak, MR & Hoque, ME 2015, 'A Review on Pineapple Leaves Fibre and Its Composites', International Journal of Polymer Science, p. 950567.

- 52. Krysztof, M, Olejnik, K, Kulpinski, P, Erdman, A & Sasiadek, E 2021, 'A comparative study of the effect of cellulose-based deep coating and pulp refining on the structural and mechanical properties of paper', BioResources, vol. 16, no. 3, pp. 5376-5389.
- 53. Yang, X, Zhao, Z, Wang, Z, Ge, Z & Zhou, Y 2021, 'Microstructure identification based on vessel pores feature extraction of high-value hardwood species', BioResources, vol. 16, no. 3, pp. 5329-5340.
- 54. Beeckman, H 2016, 'Wood anatomy and trait-based ecology', IAWA Journal, vol. 37, no. 2, pp. 127-151.
- 55. Beroual, M., L. Boumaza, O. Mehelli, D. Trache, A. Fouzi Tarchoun, and K. Khimeche. 2021. Physicochemical properties and thermal stability of microcrystalline cellulose isolated from esparto grass using different delignification approaches. Journal of Polymers and the Environment 29 (1):130-42. doi:10.1007/s10924-020-01858-w.
- 56. Bessa, W., D. Trache, M. Derradji, and A. Fouzi Tarchoun. 2022. Kevlar fabric reinforced polybenzoxazine composites filled with silane treated microcrystalline cellulose in the interlayers: The next generation of multi-layered armor panels. Defence Technology 18 (11):2000-07. doi:10.1016/j.dt.2021.10.005.
- 57. Bhasney, S. M., K. Mondal, A. Kumar, and V. Katiyar. 2020. Effect of microcrystalline cellulose [MCC] fibres on the morphological and crystalline behaviour of high density polyethylene [HDPE]/polylactic acid [PLA] blends. Composites Science and Technology 187 (107941):1-8. doi:10.1016/j.compscitech.2019.107941.
- 58. Boudjellal, A., D. Trache, K. Khimeche, S. Lotfi Hafsaoui, and M. Seddik Razali. 2022. Preparation and characterization of graphene oxide-based natural hybrids containing alfa fibers or microcrystalline cellulose. Journal of Natural Fibers 19 (13):5321-32.

doi:10.1080/15440478.2021.1875373.

- Cataldi, A., F. Deflorian, and A. Pegoretti. 2015. Microcrystalline cellulose filled composites for wooden artwork consolidation: Application and physic-mechanical characterization. Materials & Design 83:611-19. doi:10.1016/j.matdes.2015.06.037.
- 60. Chen, J., X. Wang, Z. Long, S. Wang, J. Zhang, and L. Wang. 2020. Preparation and performance of thermoplastic starch and microcrystalline cellulose for packaging composites: Extrusion and hot pressing. International Journal of Biological Macromolecules 165:2295-302. doi:10.1016/j.ijbiomac.2020.10.117.
- 61. Collazo-Bigliardi, S., R. Ortega-Toro, and A. Chiralt Boix. 2018. Isolation and characterisation of microcrystalline cellulose and cellulose nanocrystals from coffee husk

- and comparative study with rice husk. Carbohydrate Polymers 191:205-15. doi:10.1016/j.carbpol.2018.03.022.
- 62. Darus, N., M. Tamimi, S. Tirawaty, M. Muchtazar, D. Trisyanti, R. Akib, D. Condorini, and K. Ranggi. 2020. An overview of plastic waste recycling in the urban areas of java Island in Indonesia. Journal of Environmental Science and Sustainable Development 3 (2):402-15. doi:10.7454/jessd.v3i2.1073.
- 63. Dou, Y., and D. Rodrigue. 2022. Morphological, thermal and mechanical properties of recycled HDPE foams via rotational molding. Journal of Cellular Plastics 58 (2):305-23. doi:10.1177/0021955X211013793.
- 64. Gabr, M. H., N. T. Phong, K. Okubo, K. Uzawa, I. Kimpara, and T. Fujii. 2014. Thermal and mechanical properties of electrospun nano-cellulose reinforced epoxy nanocomposites. Polymer Testing 37:51-58. doi:10.1016/j.polymertesting.2014.04.010.
- 65. Gao, S. L., and J. Kyo Kim. 2000. Cooling rate influences in carbon fibre/PEEK composites.
- Part 1. Crystallinity and interface adhesion. Composites Part A, Applied Science and Manufacturing 31 (6):517-30. doi:10.1016/S1359-835X(00)00009-9.
- Haafiz, M. K. M., A. Hassan, I. M. I. Zzainoha Zakaria, M. S. Islam, M. Jawaid, and M. Jawaid. 2013. Properties of polylactic acid composites reinforced with oil palm biomass microcrystalline cellulose. Carbohydrate Polymers 98:139-45. doi:10.1016/j.carbpol.2013.05.069.
- 67. Hong, S. H., and S. Ho Hwang. 2021. Enhancing the mechanical performance of surfacemodified microcrystalline cellulose reinforced high-density polyethylene composites. Materials Today Communications 27 (102426):1-6. doi:10.1016/j.mtcomm.2021.102426.
- 68. Jabbar, A., J. Militký, J. Wiener, B. Madhukar Kale, U. Ali, and S. Rwawiire. 2017.

 Nanocellulose coated woven jute/green epoxy composites: Characterization of mechanical and dynamic mechanical behavior. Composite Structures 161:340-49.

 doi:10.1016/j.compstruct.2016.11.062.
- 69. Karakus, K., İ. Atar, İ. Halil Basboga, F. Bozkurt, and F. Mengleloglu. 2017. Wood ash and microcrystalline cellulose (MCC) filled unsaturated polyester composites. Kastamonu University Journal of Forestry Faculty 17 (2):282-89. doi:10.17475/kastorman.297702.
- Kiziltas, A., D. J. Gardner, Y. Han, and H. Seung Yang. 2014. Mechanical properties of microcrystalline cellulose (MCC) filled engineering thermoplastic composites. Journal of Polymers and the Environment 22 (3):365-72. doi:10.1007/s10924-014-0676-5.

- 71. Koniuszewska, A. G., and J. W. Kaczmar. 2016. Application of polymer based composite materials in transportation. Progress in Rubber, Plastics and Recycling Technology 32 (1):1-23. doi:10.1177/147776061603200101.
- 72. Lazrak, C., B. Kabouchi, and M. Hammi. 2019. Case studies in construction materials structural study of maritime pine wood and recycled high-density polyethylene (hdper) plastic composite using infrared-atr spectroscopy, X-ray diffraction, sem and contact angle measurements. Case Studies in Construction Materials 10 (e00227):1-11.
- 73. Lei, Y., W. Qinglin, Y. Fei, and X. Yanjun. 2007. Preparation and properties of recycled HDPE/natural fiber composites. Composites Part A, Applied Science and Manufacturing 38 (7):1664-74. doi:10.1016/j.compositesa.2007.02.001.
- 74. Mathew, A. P., K. Oksman, and M. Sain. 2005. Mechanical properties of biodegradable composites from Poly Lactic Acid (PLA) and microcrystalline cellulose (MCC). Journal of Applied Polymer Science 97 (5):2014-25. doi:10.1002/app.21779.
- 75. Mubarak, Y. A. 2018. Tensile and impact properties of microcrystalline cellulose nanoclay polypropylene composites. International Journal of Polymer Science 2018:1-14. doi:10.1155/2018/1708695.
- Mubarak, Y. A., and R. Talal Abdulsamad. 2019. Effects of microcrystalline cellulose on the mechanical properties of low-density polyethylene composites. Journal of Thermoplastic Composite Materials 32 (3):297-311. doi:10.1177/0892705717753056.
- 77. Pichandi, S., S. Rana, S. Parveen, and R. Fangueiro. 2018. A green approach of improving interface and performance of plant fibre composites using microcrystalline cellulose.
- Carbohydrate Polymers 197:137-46. doi:10.1016/j.carbpol.2018.05.074.
- 78. Radzi, A. M., S. M. Sapuan, M. Jawaid, and M. R. Mansor. 2019. Effect of alkaline treatment on mechanical, physical and thermal properties of roselle/sugar palm fiber reinforced thermoplastic polyurethane hybrid composites. Fibers and Polymers 20 (4):847-55. doi:10.1007/s12221-019-1061-8.
- 79. Raharjo, W. W., R. Soenoko, Y. Surya Irawan, and A. Suprapto. 2018. The influence of chemical treatments on cantala fiber properties and interfacial bonding of cantala fiber/recycled high density polyethylene (RHDPE). Journal of Natural Fibers 15 (1):98-111. doi:10.1080/15440478.2017.1321512.
- 80. Rehman, M. M., M. Zeeshan, K. Shaker, and Y. Nawab. 2019. Effect of micro-crystalline cellulose particles on mechanical properties of alkaline treated jute fabric reinforced green epoxy composite. Cellulose 26 (17):9057-69. doi:10.1007/s10570-019-02679-4.
- 81. Reza, A., A. Hassan, M. K. Mohamad Haafiz, Z. Zakaria, and I. M. Inuwa. 2014.

Characterization of polylactic acid/microcrystalline cellulose/montmorillonite hybrid composites. Malaysian Journal of Analytical Sciences 18 (December):642-50.

82. Saiello, S., J. Kenny, and L. Nicolais. 1990. Interface morphology of carbon fibre/PEEK composites. Journal of Materials Science 25:3493-96. doi:10.1007/BF00575375.